Journal of Palaeogeography

REVIEW Open Access

The formation of authigenic deposits during Paleogene warm climatic intervals: a review

Santanu Banerjee[1*], Tathagata Roy Choudhury[1], Pratul Kumar Saraswati[1] and Sonal Khanolkar[2]

Abstract

Although Paleogene warm climatic intervals have received considerable attention for atmospheric and oceanographic changes, the authigenic mineralization associated with these time spans remains overlooked. An extensive review of the literature reveals a close correspondence between the high abundance of glauconite and warm climatic intervals during the Paleogene period. The abundance of phosphorite, ironstone, lignite and black shale deposits reveals similar trends. Although investigated thoroughly, the origin of these authigenic deposits is never understood in the background of Paleogene warming climatic intervals. A combination of factors like warm seawater, hypoxic shelf, low rate of sedimentation, and enhanced rate of continental weathering facilitated the glauconitization. The last factor caused the excess supply of nutrients, including Fe, Si, K, Mg and Al through the rivers, the cations needed for the formation of glauconite. The excessive inflow of nutrient-rich freshwater into the shallow seas further ensured high organic productivity and stratification in shallow shelves, causing hypoxia. The consequent rapid rise in sea-level during the warm periods created extensive low-relief shallow marine shelves starved in sediments. Oxygen-deficiency in the shallow marine environment facilitated the fixation of Fe into the glauconite structure. The inflow of nutrient-rich water during the warm climatic intervals facilitated the formation of phosphorite, ironstone, and organic-matter-rich sedimentary deposits as well. Although global factors primarily controlled the formation of these authigenic deposits, local factors played significant roles in some of the deposits. Therefore, phosphorites formed in marine conditions with open circulation within the tropical zone. While lush growth of rainforest covers in the tropical belt facilitated the formation of coastal lignite.

Keywords: Warm climatic intervals, Hyperthermal events, Glauconite, Phosphorite, Oolitic ironstone, Lignite, Hypoxia, Paleogene

1 Introduction

The Paleogene period witnessed several global hyperthermal events (Zachos et al. 2001). Out of them, the most significant had been that took place at the end of the late Paleocene and the beginning of early Eocene intervals when the seawater temperature rose by about 4 °C (Jenkyns 2003; Hessler et al. 2017). These hyperthermal events were triggered by an enhanced supply of greenhouse gases that ushered rapid evolutionary and/or environmental turnovers. These events are marked by records of sharp sea-level rise, ocean deoxygenation (Sluijs et al. 2014 and references therein), shoaling of the calcite compensation depth (CCD), enhanced hydrological and weathering cycles (Nicolo et al. 2007) and increased supply of kaolinite to the marine realm (Gibson et al. 2000 and references therein). Several studies link the formation of authigenic minerals to sea-level changes in sequence stratigraphic context (Morad et al. 2012). On the contrary, the role of seawater temperature and composition on authigenic mineral formation representing the 'greenhouse world' is rarely investigated beyond carbonate sediments. This paper finds a correlation of authigenic mineralization with the fluctuations in global seawater temperature. It points out marked enhancement in authigenic

* Correspondence: santanu@iitb.ac.in
[1]Department of Earth Sciences, Indian Institute of Technology Bombay, Powai, Mumbai 400076, India
Full list of author information is available at the end of the article

mineralization in marine sediments during Paleogene warm climatic intervals.

Glauconite formed abundantly during the Paleogene, constituting up to 24% of the total record (Banerjee et al. 2016a). Recently Bansal et al. (2019) attributed the high abundance of glauconite in the Upper Cretaceous to a combination of factors like high sea-level, enhanced continental weathering in warm and humid climatic conditions and oxygen depletion on shelf seas. However, because of the lack of biostratigraphic control, these authors could not relate the abundance of the Upper Cretaceous glauconites to specific geological events. Therefore, it is unclear whether the glauconite is distributed evenly within the Late Cretaceous, or it is restricted to specific time intervals. Palaeo-oceanographic conditions of the Late Cretaceous time largely continued in the Paleogene (Jenkyns 2003). The biostratigraphically constrained sections in the Paleogene provide an opportunity to explore whether the occurrence of glauconite depended on subtle changes in palaeo-oceanographic conditions corresponding to warm climatic intervals. Phosphorite is a common associate of the Late Cretaceous glauconites, particularly Tethyan deposits (Banerjee et al. 2019). Lignite, phosphorite, and ironstone deposits of commercial importance are well known in the Paleogene sedimentary succession. However, the relationship between the abundance of these minerals and hyperthermal events is never investigated. This paper aims to present the commonalities of authigenic minerals formed during the Paleogene warm climatic intervals. Although the focus of this study is on glauconitization, phosphorite, ironstone, and lignite formation are also considered. To this effect, a thorough review has been presented.

2 Global record of hyperthermal events

Paleogene time represents a complex evolution of Earth's climate bracketed within the overall warmer Cretaceous to colder Neogene transition (Zachos et al. 1993). Deep-sea benthic foraminiferal $\delta^{18}O$ and $\delta^{13}C$ values reveal extreme warming during the Paleogene (Zachos et al. 2001). Short-lived (~ 200 kyr) events of rapid climatic shifts characterize the Paleogene climate. The 'hyperthermal' events coincide with negative carbon isotopic excursions (CIEs) (Fig. 1; Cramer et al. 2003; Nicolo et al. 2007; Stap et al. 2009; Zachos et al. 2010). The negative CIE implies a rapid delivery of isotopically depleted carbon into marine shelves and the rise of pCO_2 in the atmosphere subsequently. The climatic transitions during the Paleogene had a severe impact on the biosphere and lithosphere. Microfossil records show severe decline and diversifications in pelagic and open marine ecosystems during these thermal events (e.g., Thomas 1998; Crouch et al. 2001; Kelly 2002; Khanolkar and Saraswati 2019).

Early Paleogene time records warming of Earth's surface in the period from late Paleocene (ca. 59 Ma) to early Eocene (ca. 52 Ma). Most of the hyperthermal events viz. the Paleocene–Eocene thermal maximum (PETM) or H-1 (Cramer et al. 2003) and the Eocene thermal maximum 2 (ETM2) or Eocene layers of mysterious origin (ELMO) (Lourens et al. 2005) and the Eocene thermal maximum 3 (ETM3) or H2 or "X" event (Nicolo et al. 2007; Stap et al. 2010; Zachos et al. 2010), besides several short-lived climatic perturbations viz. I1 and I2 (Cramer et al. 2003; Nicolo et al. 2007), belong to this period. These hyperthermal events belong to three warm climatic intervals (Fig. 1). The early Paleogene warming interval includes the early late Paleocene event (ELPE, Bralower et al. 2002), also known as mid-Paleocene biotic event (MPBE, Bernaola et al. 2007), and the latest Danian event (LDE, Bornemann et al. 2009) in the Paleocene, and PETM, ETM2, ETM3 and EECO (early Eocene climatic optimum) in the early Eocene. A 17 Myr of cooling trend succeeds upwards and is interrupted by another warm climatic interval incorporating the middle Eocene climatic optimum (MECO) during the early Bartonian (Fig. 1). It is followed upwards by a long-term cooling trend that continues till the early Oligocene, as the arctic ice-sheets formed. A short-lived warming interval incorporates the late Oligocene warming event (LOWE), representing the last hyperthermal event during the Paleogene (Zachos et al. 2001). The Paleocene hyperthermal events viz. Dan C2-event, latest Danian event (LDE), and early late Paleocene event (ELPE) have received less attention compared to the hyperthermal events in the Eocene (Schulte et al. 2013).

3 Paleogene authigenic mineral formation

3.1 Occurrence of glauconite

Our study presents 124 Paleogene glauconite occurrences that formed principally in four major continents/zones, and these account for > 90% of the total global record of this time (Table 1; Fig. 2). These zones are: A) North American continental margin (eastern and western coastal plain deposits); B) Palaeo-Tethys, including northern Africa, parts of southern Europe, Middle East and India to the east; C) Palaeo-North Sea, extending from the United Kingdom to the west to northern Germany in the east; and D) High southern latitudes, including New Zealand eastern Tasman Plateau and Argentina (Figs. 2, 3, 4, 5, 6). Paleogene glauconite also occurs in places in Africa, including Ivory Coast, Nigeria and South Africa, and Asia, including Russia, China and Japan. The majority of the glauconite deposits formed on the well-developed continental margin on the northern hemisphere.

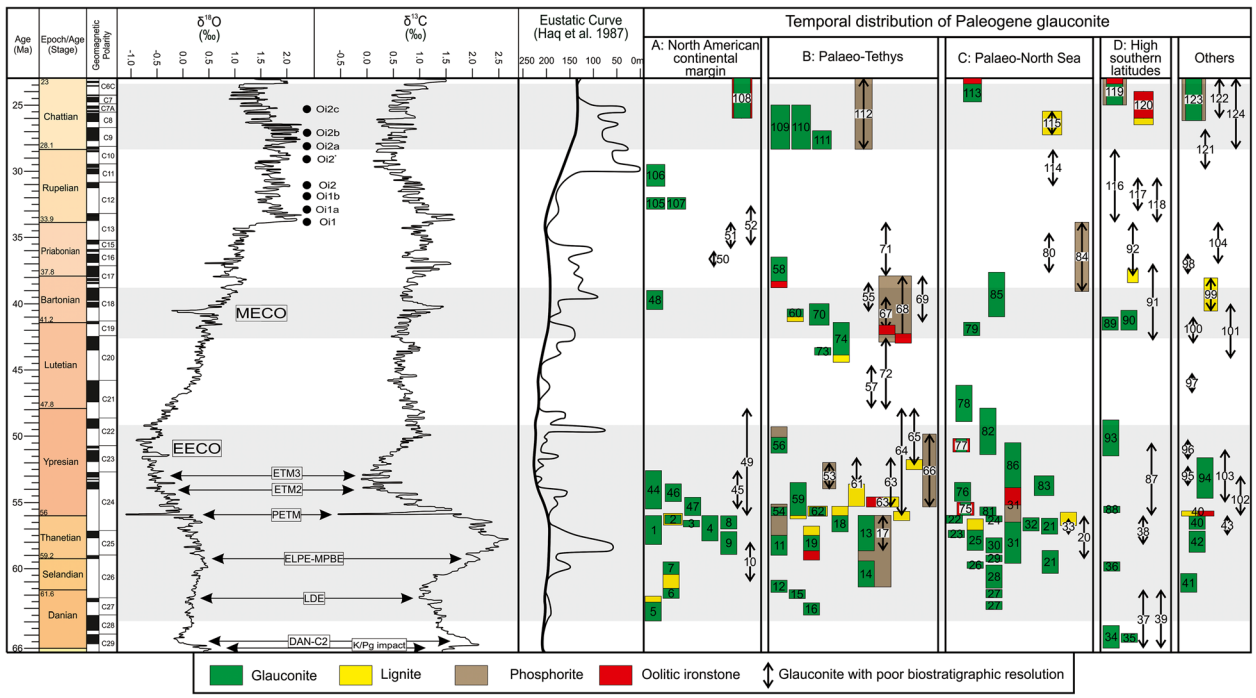

Fig. 1 Temporal distribution of Paleogene glauconite, lignite, phosphorite and oolitic ironstone in different geographic zones (right). Green rectangles indicate glauconites with precise biostratigraphic information while the vertical black arrows indicate glauconite without precise age control. Yellow, brown and red rectangles indicate age range of lignite, phosphorite and ironstone, respectively. Note overlapping of data in a few cases. The number corresponds to those provided in Table 1. Further note that most glauconite deposits occur within three warm climatic intervals marked by grey bands, separated by cooling intervals (white bands). The grey bands also incorporate lignite, phosphorite and oolitic ironstone. Also note that the early Paleogene, i.e. from early late Paleocene (Selandian) to later part of early Eocene (Ypresian), contain the highest number of glauconite deposits. The 'hyperthermal' events within the grey bands are marked along with the carbon and oxygen isotopic curves. The sea-level cycle is adapted from Haq et al. (1987). Numbers correspond to those provided in Table 1. MECO: Middle Eocene climatic optimum; EECO: Early Eocene climatic optimum; ETM2: Eocene thermal maximum 2; ETM3: Eocene thermal maximum 3; PETM: Paleocene–Eocene thermal maximum; ELPE: Early late Paleocene event; MPBE: Mid Paleocene biotic event; LDE: Latest Danian event; MPBE: Mid Paleocene biotic event; DAN-C2 represents two short-lived carbon and oxygen isotope excursion at the early Danian (Gradstein et al. 2012); Black solid circless with 'Oi' represents Oligocene isotope excursion events (Miller et al. 2009)

Out of 124 occurrences, approximately ~ 55% have reliable age control, biostratigraphic or radiometric. Therefore, they are presented separately from those not having similar age constraints in Fig. 1. The stratigraphic distribution of glauconite during the Paleogene shows a non-uniform trend (Fig. 1). Eocene, Paleocene, and Oligocene record 49%, 35%, and 16%, respectively, of total glauconite occurrences (Table 1; Fig. 1). These time intervals also included the hyperthermal events of the Paleogene (Fig. 1). The occurrence of the age-constrained glauconites coincides with three bands of warm climatic intervals discussed earlier, while the cooler intervals alternating with them have negligible glauconite occurrences (Fig. 1).

3.2 Glauconite–phosphorite association

Phosphorite deposits of economic significance are associated with glauconitic sandstone, siltstone and shale (Banerjee et al. 2019 and references therein; Boukhalfa et al. 2020). Our study reveals a cluster of glauconite–phosphorite deposits along the palaeo-Tethyan margins (Figs. 2, 3, 4, 5; see also Soudry et al. 2006). The co-occurrence of glauconite and phosphorite is reported in 17 cases, all of which correspond to the Paleogene warm climatic intervals (Fig. 1).

Extensive Paleocene–early Eocene phosphorite deposits occur along the northern margin of the African continent (Lucas and Prévôt-Lucas 1995; Soudry et al. 2006; Kechiched et al. 2018) (Figs. 3, 4). These deposits represent the so-called 'Tethyan phosphorites' (Soudry et al. 2006). Broadly similar lithology defined by clays, marls, dolomite, and foraminiferal limestone hosts phosphorites in these basins. Phosphorites deposited in low palaeo-latitudes (< 30°) in Tunisia and Algeria (Kouwenhoven et al. 1997; Messadi et al. 2016; Garnit et al. 2017; Kechiched et al. 2018) (Fig. 3). During the early Eocene, phosphorite-rich sediments, hosting glauconite, extended towards the north in shallow marine deposits of Germany (Dill et al. 1996), and to the east in Dababiya Quarry Member in Egypt (Metwally and Mahfouz 2018) (Fig. 4). During the middle to late Eocene, the locus of

Table 1 Paleogene glauconites along with precise age, associated lithology, mineral and biostratigraphic assemblage (the serial no. of data correspond to those provided in Figs. 1, 2, 3, 4, 5, 6)

Serial no.	Author	Age / Stratigraphic unit, location	Lithology	Depositional environments	Biostratigraphic details	Associated authigenic phases
PALEOCENE						
A: North American continental margin						
1	Stassen et al. (2015)	Paleocene / Vincetown Formation, New Jersey Gulf Coastal Plain, USA	Glauconitic quartz sand	Middle to outer neritic	Glauconite-bearing Vincetown Formation was deposited during NP9a. The lithology changed to a kaolinite-rich mudstone with the onset of PETM	The glauconite-bearing sandy unit is overlain by a transitional bed deposited during PETM
2	Sluijs et al. (2014)	Paleocene / Tuscahoma Formation, Wilcox Group, Gulf Coastal Plain, USA	Glauconitic sands and silts	Shallow marine to estuarine	Glauconitic unit demarcates *Apectodinium* acme and shallow marine dys-oxic condition	Lignite appears intermittently within the formation
3	John et al. (2008)	Paleocene / Moreno Formation, Tumley Gulch Section, USA	Glauconitic shale	Outer Shelf	Glauconitic unit was deposited during NP9	
4	Cramer et al. (1999)	Paleocene / Vincetown Formation, ODP Leg 174AX, USA	Glauconitic sand (> 40% sand)	Shallow marine	Glauconitic sand was deposited during NP9a	
5	Liu et al. (1997)	Paleocene / Hornerstown Formation, ODP Leg 150X, USA	Quartzose glauconitic clay	Middle neritic	Glauconite formation took place during biozone P1c or NP3	Lignite appears at the top part of the section
6	Mancini and Tew (1993)	Paleocene / Matthews Landing Marl Member, Porters Creek Formation, USA	Fossiliferous sandstone and marlstone	Shallow marine	In Porters Creek Formation, glauconite is confined within lower part of *M. angulata* I.Z (upper part of NP4 toward the boundary of NP4–NP5)	
7	Mancini and Tew (1993)	Paleocene / Coal Bluff Member, Naheola Formation, USA	Fossiliferous sandstone and marlstone	Shallow shelf	In Naheola Formation, glauconite is confined within *P. pusilla pusilla* I.Z (Upper NP5)	The glauconitic sandstones and marlstones overlie a lignitic marlstone member, which grades laterally into carbonaceous shale
8	Self-Trail et al. (2012)	Paleocene / Aquia Formation, USA	Glauconitic sandstone	Shallow shelf	Glauconitic Aquia Formation was deposited during NP9a and truncated by unconformity at Paleocene–Eocene boundary	
9	Mancini (1981)	Paleocene / Nanafalia Formation, USA	Glauconitic sandstone	Shallow shelf	Biostratigraphically the Middle Member belongs to *M. pusilla pusilla* I.Z. and Grampian Hill belongs to *P. pseudomenadrii* R.Z.	
10	Duarte and Martínez (2002)	Paleocene / Sepultura Formation, Mexico	Glauconitic sandstone with ovoid and vermiform pellets	Shallow marine	Absolute K–Ar ages of glauconite are 59 ± 1 Ma and 60 ± 1 Ma. Although biostratigraphy not given, author reports that the ages are consistent with reported biostratigraphic age	
B: Palaeo-Tethys (northern Africa, southern Europe and eastern Tethys)						
11	Kouwenhoven et al. (1997)	Paleocene / El Kef section, El Haria Formation, Tunisia	Siltstone	Middle to inner neritic setting	Glauconitic unit is dated with planktonic foraminifera and calcareous nannoplankton to be of NP6/7–NP7/8 age	At the basal part, close to K–Pg boundary, pyrite is associated. Phosphorite occurs at the

Table 1 Paleogene glauconites along with precise age, associated lithology, mineral and biostratigraphic assemblage (the serial no. of data correspond to those provided in Figs. 1, 2, 3, 4, 5, 6) *(Continued)*

Serial no.	Author	Age / Stratigraphic unit, location	Lithology	Depositional environments	Biostratigraphic details	Associated authigenic phases
						upper part
12	Sprong et al. (2013)	Paleocene / Sidi Nasseur Section, El Haria Formation, Tunisia	Marl	Shallow marine	Glauconite beds of P3a/P3b age serves as a marker bed to the latest Danian event (LDE) along the Tunisian deposits	
13	Garnit et al. (2017)	Paleocene / Chouabine Formation, Metlaoui Group, Tunisia	Glauconite associated with phosphorite	Shallow marine	Precise biostratigraphy not provided	Restricted marine condition in Eastern Basin and Gafsa-Metlaoui Basin inhibited glauconite formation and favoured phosphorite deposit. Open ocean condition in Northern Basin favoured phosphorite with abundant glauconite
14	Messadi et al. (2016)	Paleocene / Thelja Formation, Southern Tunisia	Glauconite associated with phosphorite	Shallow marine	Precise biostratigraphy not provided	Glauconites are associated with phosphates
15	Steurbaut et al. (2000)	Paleocene / Aïn Settara marls, El Haria Formation, Tunisia	Marl	Shallow marine	Glauconite bed is assigned to subzone NTp7B	
16	Speijer and Schmitz (1998)	Paleocene / Dhakla Formation, Egypt	Conglomeratic and glauconitic marl	Palaeodepth varies at ~ 200 m	Planktonic foraminiferal zone P1c was assigned to the glauconitic marl	
17	Kechiched et al. (2018)	Paleocene / Djebel el Kouif and Kef Essenoun deposit, Algeria	Argillaceous phosphorite	Shallow marine	Precise biostratigraphy not provided	Associated with phosphorite deposits, glauconites are concentrated in the phosphorite-rich bands
18	Samanta et al. (2013a)	Paleocene / Cambay Shale Formation, India	Shale	Lagoonal	Ar–Ar age of glauconite is 56.6 ± 0.7 Ma	Lignite appears as thick seams within a dominantly shaley lithology
19	Egger et al. (2009)	Paleocene / Kroischbach Member, Kressenberg Formation, Austria	Glauconite-bearing quartz sandstone	Shallow marine	Glauconite-bearing quartz sandstone unit was deposited during upper Thanetian (NP8)	Coal-bearing terrestrial deposits of the Paleogene Holzer Formation yielded palynoflora typical of *Nypa* mangrove forest. Ooidal sandstone unit is present at the basal part of the section
C: Palaeo-North Sea						
20	Knox (1979)	Paleocene / Thanet Beds, England	Glauconitic clayey sandstone	Shallow marine	Precise biostratigraphy not provided	The high degree of montmorillonite in most of the 'glauconite' pellets is correlated to the montmorillonite-rich nature of associated clays or even to a pyroclastic mud precursor.

Table 1 Paleogene glauconites along with precise age, associated lithology, mineral and biostratigraphic assemblage (the serial no. of data correspond to those provided in Figs. 1, 2, 3, 4, 5, 6) *(Continued)*

Serial no.	Author	Age / Stratigraphic unit, location	Lithology	Depositional environments	Biostratigraphic details	Associated authigenic phases
21	Fitch et al. (1978)	Paleocene / Oldhaven Beds, Thanet Sand England	Sandstone	Shallow marine	Fair age of Thanet Bed and Reculver Sand obtained by K–Ar method. Basal Thanet Sand: 59.5 ± 0.9 Ma; Reculver Sand: 56.8 ± 0.6 Ma. Precise biostratigraphy not provided	
22	Huggett et al. (2017)	Paleocene / Upnor Formation, England	Fine- to medium-grained sandstone with glauconite pellets	Shallow marine to estuarine	Age of glauconite formation is ~ 55.6–56.2 Ma (NP8–NP9) which is referred to Ali and Jolley (1996)	
23	Ellison et al. (1996)	Paleocene / Upnor Formation, England	Medium-grained, glauconitic, quartzose sands	Shallow marine	C25n to C24r, NP9, Dinocyst zone *A. hyperacanthum*; FO *Discoaster multiradiatus* Four (4) pulses of glauconite formation is observed and dated magnetostratigraphically to be in between C25n to C24r	
24	Schmitz et al. (2004)	Paleocene / Ølst Fm., Østerrenden core, Denmark	Siltstone	Shallow marine	Glauconitic siltstone appears just below the peak-CIE i.e. *Apectodinium* acme	Presence of ash layer directly points towards explosive basaltic volcanism
25	Steurbaut et al. (2003)	Paleocene / Grandglise Sand Member, Hannut Formation, Belgium	Bioturbated sandstone, very fine sand to sandy silt	Shallow marine	Just below the main CIE, reappears again in 54.6 Ma in Mont Héribu Clay Member. Before CIE – Hannut Formation, in sandstone, upper part of NP8	Tienen Formation, sandwiched between Hannut Formation and Mont Héribu Clay Member have abundant thin lignite bodies
26	Clemmensen and Thomsen (2005)	Paleocene / Lellinge Greensand Formation, North Sea Basin	Greensand	Inner shelf	Lellinge Greensand deposited during 59.5–60 Ma. Biostratigraphic information is based on calcareous nannoplankton and supplemented by planktonic foraminifera	
27	Hamberg et al. (2005)	Paleocene / Bohr Member, Vále Formation, Siri Canyon, Stavanger Platform Area, Denmark	Sandstone	Deep marine	Biostratigraphic data provided. All Paleogene sandstones in Siri Canyon, Denmark contains glauconite	
28	Hamberg et al. (2005)	Paleocene / Ty Member, Vile Formation, Siri Canyon, Stavanger Platform Area, Denmark	Sandstone	Deep marine	Biostratigraphic data provided	
29	Hamberg et al. (2005)	Paleocene / Heimdal Member, Holmehus Formation, Siri Canyon, Stavanger Platform Area, Denmark	Sandstone	Deep marine	Biostratigraphic data provided	
30	Hamberg et al. (2005)	Paleocene / Heimdal Member, Lista Formation, Siri Canyon, Stavanger Platform Area, Denmark	Sandstone	Deep marine	Biostratigraphic data provided	
31	Dill et al. (1996)	Paleocene / Formation A, North German Basin, Germany	Sandstone	Shallow marine	Biostratigraphic data provided, dinocyst zone D4 is assigned for Formation A	Glauconite is confined within the lower sandstones. Glauconite-rich Formation A is overlain by phosphorite and

Table 1 Paleogene glauconites along with precise age, associated lithology, mineral and biostratigraphic assemblage (the serial no. of data correspond to those provided in Figs. 1, 2, 3, 4, 5, 6) *(Continued)*

Serial no.	Author	Age / Stratigraphic unit, location	Lithology	Depositional environments	Biostratigraphic details	Associated authigenic phases
						sideritic horizon of Formation B
32	Schmitz et al. (2004)	Paleocene / Zumaya and Ermua Section, Basque Basin, Spain	Grey limestone with glauconite at the top	Middle to lower bathyal: shallow marine	Glauconitic limestone appears just below the peak-CIE i.e. *Apectodinium* acme The limestone bed is assigned to NP9 zone.	
33	Dypvik et al. (2011)	Paleocene / Frysjaodden Formation, Norway	Highly-bioturbated sandstone	Deep marine	Precise biostratigraphy not provided. Report of PETM is based on Th/U and clay mineral proxies	Coal seams are present in the upper part of the formation. PETM interval contains abundant pyrite
D: High southern latitudes						
34	Ferrow et al. (2011)	Paleocene / Conway Formation, New Zealand	Sandstone	Shallow marine	Glauconite is present throughout the formation, in Paleogene it is associated with *Trithyrodinium evittii* l.Z,	In K-Pg boundary, jarosite is associated Fe-bearing phases. Sporadic coal seams are present
35	Hines et al. (2013)	Paleocene / Awhea Formation, New Zealand	Glauconitic sandstone	Deep marine	Awhea Formation: Middle and upper member contain definitive Paleocene (Teurian) assemblages, including *Stensioina beccariiformis*, *Nuttallinella florealis*, *Acarinina spp.* and *Globigerina sp.*	Pyrite occurs within burrows
36	Hines et al. (2013)	Paleocene / Mungaroa Limestone, New Zealand	Glauconitic sandstone	Deep marine	Mungaroa Limestone: Calcareous nannofossil assemblages from the middle member of the Mungaroa Limestone in the Pukemuri Stream include *F. tympaniformus* and *Heliolithus cantabriae* with a notable absence of *Heliolithus kleinpellii*, placing the middle member in Upper Zone NP5.	
37	Lurcock and Wilson (2013)	Paleocene / Abbotsford Formation, New Zealand	Greensand	Shallow marine	Precise biostratigraphy not provided	Magnetite is associated/embedded in glauconite pellets
38	Schiøler et al. (2010)	Paleocene / Tartan Formation, New Zealand	Glauconitic mudstone	Marginal marine	Precise biostratigraphy not provided	
39	Franzosi et al. (2014)	Paleocene / Salamanca Formation, Argentina	Moderately sorted and weakly consolidated sand	Shallow marine	Precise biostratigraphy not provided	Volcanic clasts and glass sherds are common within the sand that hosts glauconite
Others						
40	Frieling et al. (2014)	Paleocene / Lyulinvor Formation, Russia	Sandstone	Shallow marine (from Rudmin et al. 2017)	Biostratigraphic data provided. Glauconite-rich unit separates the top of Chron 25n and the PETM	In the eastern part, a sapropelic unit overlies the glauconite. In the western part, thicker glauconitic sandstone overlain by oolitic ironstone
41	Iakovleva and Kulkova (2003)	Paleocene / Talitskaya Formation, West Siberia	Glauconitic sandstone and siltstone	Shallow marine	Glauconite-bearing sediments range in age from P3b to middle P7. Glauconite	

Table 1 Paleogene glauconites along with precise age, associated lithology, mineral and biostratigraphic assemblage (the serial no. of data correspond to those provided in Figs. 1, 2, 3, 4, 5, 6) *(Continued)*

Serial no.	Author	Age / Stratigraphic unit, location	Lithology	Depositional environments	Biostratigraphic details	Associated authigenic phases
					occurs within the dinoflagellate zone *Cerodinium speciosum* (D3 pars)	
42	Iakovleva and Kulkova (2003)	Paleocene / Serovskaya Formation, West Siberia	Glauconitic sandstone	Shallow marine	Glauconite is confined within the dinoflagellate zone *Alisocysta margarita* (D4 pars)	
43	Nahon et al. (1980)	Paleocene / Eboinda region, Ivory Coast	Shale	Shallow marine	Precise biostratigraphy not provided	Diagenetic pyrite replaces many glauconite. Glauconitic beds alternate with black shale
EOCENE						
A: North American continental margin						
44	Stassen et al. (2015)	Eocene / Manasquan Formation, New Jersey Gulf Coastal Plain, USA	Fine sand/silt	Shallow marine	Biostratigraphic data provided	
45	Goodman (1979); Gibson et al. (1993)	Eocene / Nanjemoy Formation, Northern Gulf Coastal Plain, USA	Fine-grained quartz sand	Shallow marine	Precise biostratigraphy not provided	
46	John et al. (2008)	Eocene / Lodo Formation, USA	Fine sandstone	Outer shelf	Gulch sections: Glauconite appears at base of unconformity at NP10–NP11 truncating the PETM recovery deposits and at latter part of NP12	
47	Sluijs et al. (2014)	Eocene / Bashi Marl Member, Hatchetigbee Formation, USA	Coarse sandstone	Inner shelf	Biostratigraphy (in parts) is provided	Burst (1958) and Hower (1961) characterized the glauconites
48	Pietsch et al. (2016)	Eocene / Gosport Sand Alabama Gulf Coastal Plain, USA	Sandstone	Shallow marine	Biostratigraphic data provided	
49	Strickler and Ferrell Jr. (1990)	Eocene / Wilcox Sandstone, USA / Lower Eocene, Texas, USA	Glauconitic lithic arkose / feldspathic litharenite with pellets	Shallow marine	Glauconite is in lower Eocene Wilcox Group but no biostratigraphic or radiogenic dates are given. Precise biostratigraphy not provided	
50	Harris et al. (1984)	Eocene / Santee Limestone (South Carolina), USA	Limestone	Shallow marine	Rb–Sr radiometric age of glauconites from Santee Limestone is 36.7 ± 0.6 Ma	
51	Harris et al. (1984)	Eocene / Castle Hayne Limestone (North Carolina), USA	Limestone	Shallow marine	Rb–Sr radiometric age of glauconites from Castle Hayne Limestone is 34.9 ± 1.1 Ma	
52	Harris et al. (1984)	Eocene / Cross Formation, USA	Impure limestone	Shallow marine	Rb–Sr radiometric age of glauconites from Cross Formation is 34.1 ± 1.5 Ma	
B: Palaeo-Tethys (northern Africa, southern Europe and eastern Tethys)						
53	Tlig et al. (2010)	Eocene / El Garia Formation, Metlaoui Group, Tunisia	Impure limestone	Shallow marine	Precise biostratigraphy not provided. Glauconite is of Ypresian age	Glauconite associated with phosphate. Background lithology is marl, black shale and clayey limestone
54	Metwally and	Eocene / Esna Formation, Dababiya	Shale	Shallow marine	Glauconite-bearing strata are marked by	Glauconite is associated with

Table 1 Paleogene glauconites along with precise age, associated lithology, mineral and biostratigraphic assemblage (the serial no. of data correspond to those provided in Figs. 1, 2, 3, 4, 5, 6) *(Continued)*

Serial no.	Author	Age / Stratigraphic unit, location	Lithology	Depositional environments	Biostratigraphic details	Associated authigenic phases
	Mahfouz (2018)	Quarry Member, Egypt			the LO of *Discoaster araneus* and/or *Rhomboaster* taxa to the LO of *Tribrachiatus bramlettei*. Also, glauconite belongs to *Acarinina sibaiyaensis* (E1) Zone	phosphates
55	Marivaux et al. (2014)	Eocene / Fortuna Formation, Tunisia	Shale	Subtidal to upper intertidal	Glauconites are of late middle Eocene (Bartonian). Radiometric ages from glauconite (in m.y.): 38.7 ± 1.0, 39.4 ± 1.1, 40.7 ± 1.1, 39.3 ± 1.0	
56	Jorry et al. (2003)	Eocene / Choubine Formation, Central Tunisia	Marl	Shallow marine	Biostratigraphy of the glauconitic marl indicates a P8 biozone	Glauconitic marl is overlain by rich phosphate deposits
57	Hegab and El-Wahed (2016)	Eocene / Qarara Formation / Middle Eocene, Egypt	Green shale with pellets	Shallow marine	Precise biostratigraphy not provided	
58	Baioumy (2007); El-Habaak et al. (2016)	Eocene / Hamra Formation, Egypt	Sandy glauconitic limestone	Marginal marine	Although the formation is biostratigraphically constrained using *Nummulite* species and SBZ. The glauconitic unit did not yield any microfossil	Glauconite in Upper Hamra Formation unconformably overlies oolitic ironstone deposits of Lower Hamra Formation
59	Chattoraj et al. (2009)	Eocene / Naredi Formation, Kutch, India	Green shale	Middle shelf	Two glauconite horizons occur within Naredi Formation, the basal unit is biostratigraphically dated as SBZ 8 and the upper bed is dated as SBZ10	Lignite is present at the basal part of the Naredi Formation
60	Banerjee et al. (2012b)	Eocene / Harudi Formation, Kutch, India	Green shale	Lagoon to shelf transition	Biostratigraphically the glauconite bed at the top of Harudi Formation is dated to be in SBZ 17	At the basal part of Harudi Formation, lignite appears as lenses
61	Samanta et al. (2013a)	Eocene / Cambay Shale Formation, India	Shale	Lagoonal	Glauconite formed related to I1/I2 event	Thick seams of lignite within a dominantly shaley lithology
62	Kalia and Kintso (2006)	Eocene / Laki Formation, Jaisalmer Basin, India	Sandy clay	Shallow marine	Glauconite is confined within *Acarinia sibayensis* zone (E1?) and reported as basal part of P5b	Lignite occurs at the Paleocene–Eocene boundary, along with glauconite and pyrite
63	Kharkwal (1966)	Eocene / Subathu Formation, Simla, India	Limestone and calcareous sandstone	Shallow marine	Precise biostratigraphy not provided	Clays are carbonaceous at the basal part, locally coal. Possible ooidal ironstone at the basal Subathu Formation
64	Sarma and Basumallick (1979)	Eocene / Sylhet Limestone, India	Limestone	Neritic	Precise biostratigraphy not provided	Coal alternate with sandstone at the basal part, followed upwards by glauconitic nummulitic limestone
65	Sarmah and Borgohain (2012)	Eocene / Narpuh Sandstone, India	Calcareous sandstone	Shallow shelf	Precise biostratigraphy not provided	Thin lenses of coal seams at the basal part
66	Shiloni et al. (1977)	Eocene / Zor'a Formation, Israel	Glauconitic chalky	Shallow marine	Precise biostratigraphy not provided	Phosphate-bearing rocks underlie

Table 1 Paleogene glauconites along with precise age, associated lithology, mineral and biostratigraphic assemblage (the serial no. of data correspond to those provided in Figs. 1, 2, 3, 4, 5, 6) *(Continued)*

Serial no.	Author	Age / Stratigraphic unit, location	Lithology	Depositional environments	Biostratigraphic details	Associated authigenic phases
			limestone			the glauconitic limestone at the top part of the formation
67	Zarasvandi et al. (2019)	Eocene / Pabdeh Formation, Iran		Shallow marine	Precise biostratigraphy not provided	Glauconite is overlain by phosphorite. REE data indicate sub-oxic to anoxic condition
68	Beavington-Penney et al. (2006)	Eocene / Seeb Formation, Oman	Wackestone, packstone	Shallow lagoonal	Precise biostratigraphy not provided	Glauconite is associated with minor phosphate and siderite
69	Clark and Robertson (2005)	Eocene / Gümüs Member, Hasangazi Formation, Turkey	Faecal pellets and infillings	Shallow shelf	Precise biostratigraphy not provided	
70	Bektemirova et al. (2018)	Eocene / Hanabad Formation, Kyzyltokoy Basin, Kyrgyzstan	Clay	Shallow marine	The basin are dated using macrofossils (bivalve) and presented in Bosboom et al. (2017)	
71	Rasser and Piller (2004)	Eocene / Helvetic Shelf, Austria	Nummulitic limestone	Shallow marine	Precise biostratigraphy not provided	
72	Cosović and Drobne (1995)	Eocene / Adriatic Carbonate Platform, Istrian Peninsula, Croatia	Wackestone, packstone	Palaeodepth as high as ~130 m	Abundant glauconite is found confined within *Alveolina stipes* and *Alveolina munieri* zone which demarcates SBZ 13/14. Precise biostratigraphy not provided	
73	Schweitzer et al. (2005)	Eocene / "Marl with crab", Istrian Peninsula, Croatia	Foraminiferal packstones	Outer ramp	P-11 biozone was identified based on *Globigerinatheka mexicana*, *Turborotalia frontosa*, *Turborotalia possagnoensis*, and *Subbotina inaequispira* for the glauconite-bearing formation	
74	Cosović et al. (2004)	Eocene / Adriatic Carbonate Platform, Istrian Peninsula, Croatia	Foraminiferal wackestone/ packstone	Slightly deeper water	Glauconite ages were determined using foraminiferal biozones. Glauconite occurs within SBZ13–SBZ16 interval	In the Liburnian Formation, the basal part of Eocene succession, coal occurs locally
C: Palaeo-North Sea						
75	Huggett and Gale (1997)	Eocene / Harwich Formation, Hampshire Basin, UK	Fine-grained glauconitic sandstone	Shallow marine	Biostratigraphic data obtained from the authors and Ali and Jolley (1996). Glauconitic sandstone belongs to NP9 and part of NP10	Siderite-bearing units alternate with glauconites. Harwich Formation contain tephra deposits
76	Huggett and Gale (1997); Amorosi and Centineo (1997)	Eocene / London Clay Formation, Hampshire Basin, UK	Fine-grained glauconitic sandstone	Shallow marine	Biostratigraphic data obtained from the authors and Ali and Jolley (1996)	
77	Huggett and Gale (1997); Amorosi and Centineo (1997)	Eocene / Wittering Formation, Hampshire Basin, UK	Glauconitic silty sand	Shallow marine	Biostratigraphic data obtained from the authors and Ali and Jolley (1996)	Two glauconitic horizons are overlain by siderite concretion-bearing units
78	Huggett and Gale (1997); Amorosi and	Eocene / Earnley Formation, Hampshire Basin, UK	Bioturbated glauconitic sand	Shallow marine	Biostratigraphic data obtained from the authors and Ali and Jolley (1996)	

Table 1 Paleogene glauconites along with precise age, associated lithology, mineral and biostratigraphic assemblage (the serial no. of data correspond to those provided in Figs. 1, 2, 3, 4, 5, 6) *(Continued)*

Serial no.	Author	Age / Stratigraphic unit, location	Lithology	Depositional environments	Biostratigraphic details	Associated authigenic phases
	Centineo (1997)					
79	Hughes and Whitehead (1987); Huggett and Gale (1997)	Eocene / Barton Clay, Hampshire Basin, UK	Glauconitic muddy silt	Shallow marine	Biostratigraphic data obtained from the authors and Ali and Jolley (1996)	
80	Huggett and Cuadros (2010)	Eocene / Headon Hill Formation, Hampshire Basin, UK	Shale, siltstones and marls	Lacustrine	Biostratigraphic zonation of Aubry (1985) indicates a NP18 to NP19–20 age of Headon Hill Formation. Radiometric dating provides ~ 34 Ma. Precise biostratigraphy not provided	
81	Steurbaut et al. (2003)	Eocene / Mont Héribu Clay Member, Belgium	Glauconitic clayey very fine sand	Mostly lagoonal	Biostratigraphic data provided	
82	Vanhove et al. (2011)	Eocene deposits of Belgium (including Tielt, Hyon, Gentbrugge & Aalatar Formation), Belgium	Glauconitic sand and muds	Shallow marine	Glauconitic sand and mud is very common in latest NP12 and NP13 zones	
83	Morton et al. (1984)	Eocene / Offshore Ireland DSDP Leg-81, North Sea Basin	Pale-green clay	Shallow marine shelf	Glauconitization started at late NP10 and truncated at NP12. Biostratigraphy and magnetostratigraphy data available	
84	Czuryłowicz et al. (2014)	Eocene / Siemeń Formation, Lubartów area, Poland	Siltstone and sandstone	Shallow marine	Precise biostratigraphy not provided	Glauconitic silty sand overlies a phosphate unit
85	Gedl (2014)	Eocene sediments of Solokija Graben, Roztocze, Poland	Glauconitic sandstone, calcareous and non-calcareous	Shallow marine	Glauconitic sands are confined from upper part of NP16 to lower NP18 or top of NP17	
86	Dill et al. (1996)	Eocene / Formation C, North German Basin, Germany	Sandstone	Shallow marine	Formation C is confined within Subzone D7a and D8nb	Glauconite is confined within the lower sandstones while pyrite formed in clays and marls
D: High southern latitudes						
87	Sorrentino et al. (2014)	Eocene / Red Bluff Tuff Formation, New Zealand	Volcanic tuff	Shallow marine	Precise biostratigraphy not provided Age of late Paleocene–early Eocene was proposed by Campbell et al. (1988)	Magnetite and hematite are associated with glauconite
88	Crouch et al. (2003)	Eocene / Wanstead Formation, Tawanui, New Zealand	Glauconitic sandy siltstone	Deep marine	Biostratigraphy is done based on *Apectodinium* acme and dinocyst assemblages	Although depositional environment was deep, land-derived terrestrial components are abundant
89	Wei (2004)	Eocene / Tasmanian Gateway, ODP Leg No 189, New Zealand	Silty claystone and siltstone	Shallow marine	Its first occurrence of glauconite is between the FO of *Reticulofenestra reticulate* (41.2 Ma) and that of *Reticulofenestra umbilicus* (42.0 Ma) and thus it can be dated as 41–42 Ma	
90	Dallanave et al. (2016)	Eocene / Ashley Mudstone, New Zealand	Mudstone	Deep marine	Age of glauconite is confined to NP16, LO of *Reticulofenestra umbilicus* marks the	

Table 1 Paleogene glauconites along with precise age, associated lithology, mineral and biostratigraphic assemblage (the serial no. of data correspond to those provided in Figs. 1, 2, 3, 4, 5, 6) *(Continued)*

Serial no.	Author	Age / Stratigraphic unit, location	Lithology	Depositional environments	Biostratigraphic details	Associated authigenic phases
					onset of glauconite but upper boundary is not defined. Absolute age of glauconite is 42.64 Ma (Gradstein et al. 2012)	
91	Aitchison (1988)	Eocene / Tapui glauconitic sandstone, New Zealand	Sandstone	Storm-dominated inner shelf	Precise biostratigraphy not provided. Glauconites are of early to middle Eocene age	
92	MacGregor (1983)	Eocene / Waitakere Limestone. Nile Group, New Zealand	Limestone	Marginal marine	Precise biostratigraphy not provided. Age is based on benthic foraminiferal assemblage but not precisely demarcated	Pyrite occurs at upper part of the section. Underlying Brunner Coal measure is a thick coal-bearing unit
93	Hines et al. (2013)	Eocene / Pukemuri Siltstone, New Zealand	Glauconitic sandstone	Deep marine	Pukemuri Siltstone: The presence of *Discoaster lodoensis* throughout the formation indicates correlation with Nannofossil Zones NP12–14	
Others						
94	Iakovleva and Kulkova (2003)	Eocene / Tavdinskaya Formation, West Siberia, Russia	Glauconitic sand and siltstone	Shallow marine	Glauconite-bearing sediments of Tavdinskaya Formation belong to *Rhombodinium draco* dinoflagellate zone	
95	Polevaya et al. (1961)	Paleogene deposits of Abkhazia, Russia	Sandstone, clayey sandstone and limestone	Shallow marine	Absolute age of glauconite by radiometric dating yields ~ 53 Ma	
96	Polevaya et al. (1961)	Paleogene deposits of Turgay, Russia	Sandstone, clayey sandstone and limestone	Shallow marine	Radiometric dating provides ~ 51 Ma	
97	Polevaya et al. (1961)	Paleogene deposits of Volga River Area, Russia	Sandstone, clayey sandstone and limestone	Shallow marine	Radiometric dating provides ~ 46 Ma is reported	
98	Polevaya et al. (1961)	Paleogene deposits of Ciscaucasia, Russia	Sandstone, clayey sandstone and limestone	Shallow marine	Radiometric dating provides ~ 37 Ma	
99	Geptner et al. (2008)	Eocene / Amanin Formation, Russia	Volcanogenic sandstone and mudstone	Shallow marine	Precise biostratigraphy not provided	
100	Wei et al. (2018)	Eocene / Shahejie Formation Bohai Bay Basin, China	In varying lithologies from sandstone to calcareous mudstone	Shallow marine	Main glauconite event took place ~ 42.47 Ma with two minor event ~ 35.99 Ma and ~ 31.94 Ma. Precise biostratigraphy not provided	
101	Jiang et al. (2007)	Eocene / Shulu Sag Basin, China	Calcareous shale and siltstone	Lacustrine	Precise biostratigraphy not provided	
102	Petters and Olsson (1979)	Eocene / Akinbo Formation, Nigeria	Shale	Shallow marine	K–Ar method yields 54.45 ± 2.7 Ma	

Table 1 Paleogene glauconites along with precise age, associated lithology, mineral and biostratigraphic assemblage (the serial no. of data correspond to those provided in Figs. 1, 2, 3, 4, 5, 6) *(Continued)*

Serial no.	Author	Age / Stratigraphic unit, location	Lithology	Depositional environments	Biostratigraphic details	Associated authigenic phases
103	Amaral (1967)	Eocene / Calumbi Formation, Mosquiro well, Sergipe-Alagoas Basin, Brazil	Glauconitic sandstone	Shallow marine	K–Ar absolute ages of glauconite from Mosquiro Formation are 53 ± 2 Ma and 51 ± 2 Ma	
104	Amaral (1967)	Eocene / Cururu well, Majaró Basin, Brazil	Fine sandstone and siltstone	Shallow marine	K–Ar absolute age of glauconite from Mosquiro Formation is 35 ± 2 Ma	
OLIGOCENE						
A: North American continental margin						
105	Miller et al. (2009)	Oligocene / Sequence O1, New Jersey Coastal Plain, USA	Glauconitic sand	Middle shelf	The Sequence O1 has rich glauconite concentration and age is defined as NP22	
106	Miller et al. (2009)	Oligocene / Sequence O2, New Jersey Coastal Plain, USA	Glauconitic sand	Middle shelf	The Sequence O2 has rich glauconite concentration and age is defined as upper part of NP23	
107	Miller et al. (2009)	Oligocene / Bumpnose sequence, SSQ section Alabama Gulf Coastal Plain, USA	Glauconitic sand	Middle shelf	The Sequence O2 has rich glauconite concentration and age is defined as upper part of NP23	
108	Hesselbo and Huggett (2001); Savrda et al. (2001)	Oligocene / Offshore New Jersey, ODP Leg 174A, USA	Mudstone and sandstone	Deep marine	Precise biostratigraphy not provided. Age estimation is based on Sr stratigraphy (Savrda et al. 2001)	Glauconite has ooidal coating of glauconitic smectite, while shallow water glauconites have cores of siderite
B: Palaeo-Tethys (northern Africa, southern Europe and eastern Tethys)						
109	Boukhalfa et al. (2015)	Oligocene / Fortuna Formation, Tunisia	Glauconitic siltstone and mudstone	Lagoonal	Glauconite forms in Chattian. Glauconite-bearing sequence is marked by biostratigraphically well-constrained upper and lower boundary	Lagoonal glauconite of Fortuna Formation overlies a Fe-, S-bearing horizon
110	Boukhalfa et al. (2015)	Oligocene / Lower Béjaoua Group, Tunisia		Shoreface–offshore transition	Glauconite-bearing sequence is marked by biostratigraphically well-constrained upper and lower boundary	
111	Banerjee et al. (2012a)	Oligocene / Maniyara Fort Formation, Kutch, India	Green shale	Lagoonal	Glauconite age is modified to the base of SBZ 22B based on foraminiferal studies	
112	Tóth et al. (2010)	Oligocene / Eger Formation, Hungary	Carbonate cemented sandstone layers	Deep sublittoral to epibathyal	Precise biostratigraphy not provided	Phosphate is associated with glauconite even as very fine particles
C: Palaeo-North Sea						
113	Rasmussen and Dybkjær (2005)	Oligocene / Brejning Clay Member, Vejle Fjord Formation, Denmark	Bioturbated greenish silty clay	Shallow marine	Overlying the glauconitic unit is characterized by common occurrences of *Deflandrea phosphoritica* and *Chiropteridium galea* (Dinocyst assemblage)	Glaucony is abundant with pyritized burrow. Glauconitic clay is overlain by silty to sandy unit with iron oolite and siderite cemented sandstone
	Porrenga (1968)	Oligocene / Kerkom sand Belgium	Thin green clay layers	Marginal marine	Precise biostratigraphy not provided	

Table 1 Paleogene glauconites along with precise age, associated lithology, mineral and biostratigraphic assemblage (the serial no. of data correspond to those provided in Figs. 1, 2, 3, 4, 5, 6) *(Continued)*

Serial no.	Author	Age / Stratigraphic unit, location	Lithology	Depositional environments	Biostratigraphic details	Associated authigenic phases
114			and lenses intercalated in sands			
115	De Man and Van Simaeys (2004)	Oligocene / Southern North Sea Basin, Belgium	Glauconitic sand	Marginal marine	Oldest time-transgressive glauconitic sand was deposited around 26.7 Ma	Coals are present in the formation, but precise stratigraphy not available
D: High southern latitudes						
116	Van der Lingen et al. (1978)	Oligocene / Oxford Chalk, New Zealand	Cross-bedded glauconitic sand with foraminiferal infillings	Shallow marine	Precise biostratigraphy not provided	
117	Lewis and Belliss (1984)	Oligocene / Gee Greensand Otekaike Limestone, New Zealand	Greensand	Inner shelf	Age of the formation is based on Harland et al. (1982); but the age is redefined again. Precise biostratigraphy not provided. Ostracoda biostratigraphy is provided in Ayress (2006)	
118	McConchie and Lewis (1978)	Oligocene / Coleridge Formation, New Zealand	Glauconitic sandstone with faecal pellets	Shallow marine	Precise biostratigraphy not provided. Oligocene glauconite belongs to early Oligocene (Whaingaroan Stage) (Harland et al. 1982)	
119	Kelly and Webb (1999)	Oligocene / Jan Juc Formation, Torquay Group, Australia	Argillaceous sandstone	Middle shelf	Foraminiferal biostratigraphy is provided in Li et al. (1999)	Pyrite, siderite, phosphate and iron oxide minerals overlie basal glauconite rich units. Glauconitic unit contains pyrite, phosphates and iron oxides, but lacks siderite
120	Dix and Parras (2014)	Oligocene / San Julián Formation, Patagonia (Argentina)	Hardground in limestone	Shallow marine	Precise biostratigraphy not provided. Age of glauconite-bearing rocks are correlated with chronostratigraphy of Gradstein et al. (2012)	Microcrystalline siderite is associated with glauconite. Glauconite overlies coal-bearing member
Others						
121	Sageman and Speed (2003)	Oligocene / Caratas Fm., Tinajitas Lst. and Los Jabilos Fm., Venezuela	Arenites with foraminiferal infillings	Shallow marine	NP24 for Glauconitic wacke; three distinct glauconitization event without proper biostratigraphic age provided. Precise biostratigraphy not provided	
122	Amaral (1967)	Oligocene / Cururu Fm., Majaró Basin, Brazil	Fine sandstone and siltstone	Shallow marine	K–Ar age of glauconite from upper part of Cururu well section is 25 ± 2 Ma which is in good agreement with biostratigraphic data according to the author	
123	Wigley and Compton (2006)	Oligocene / Upper Oligocene-Lower Miocene Calcareous unit, South Africa	Calcareous sand	Shallow marine	Glauconite formed during Upper Oligocene (25.8–27.2 Ma)	Phosphate (CFA) is associated with glauconite
124	Tazaki and Fyfe (1992)	Oligocene / Isu Bonin Forearc Basin, ODP Leg 126, Japan	Volcanogenic sandstone	Deep marine	Precise biostratigraphy not provided	Glauconite along with celadonite and graphite occurs in volcaniclastic sediments

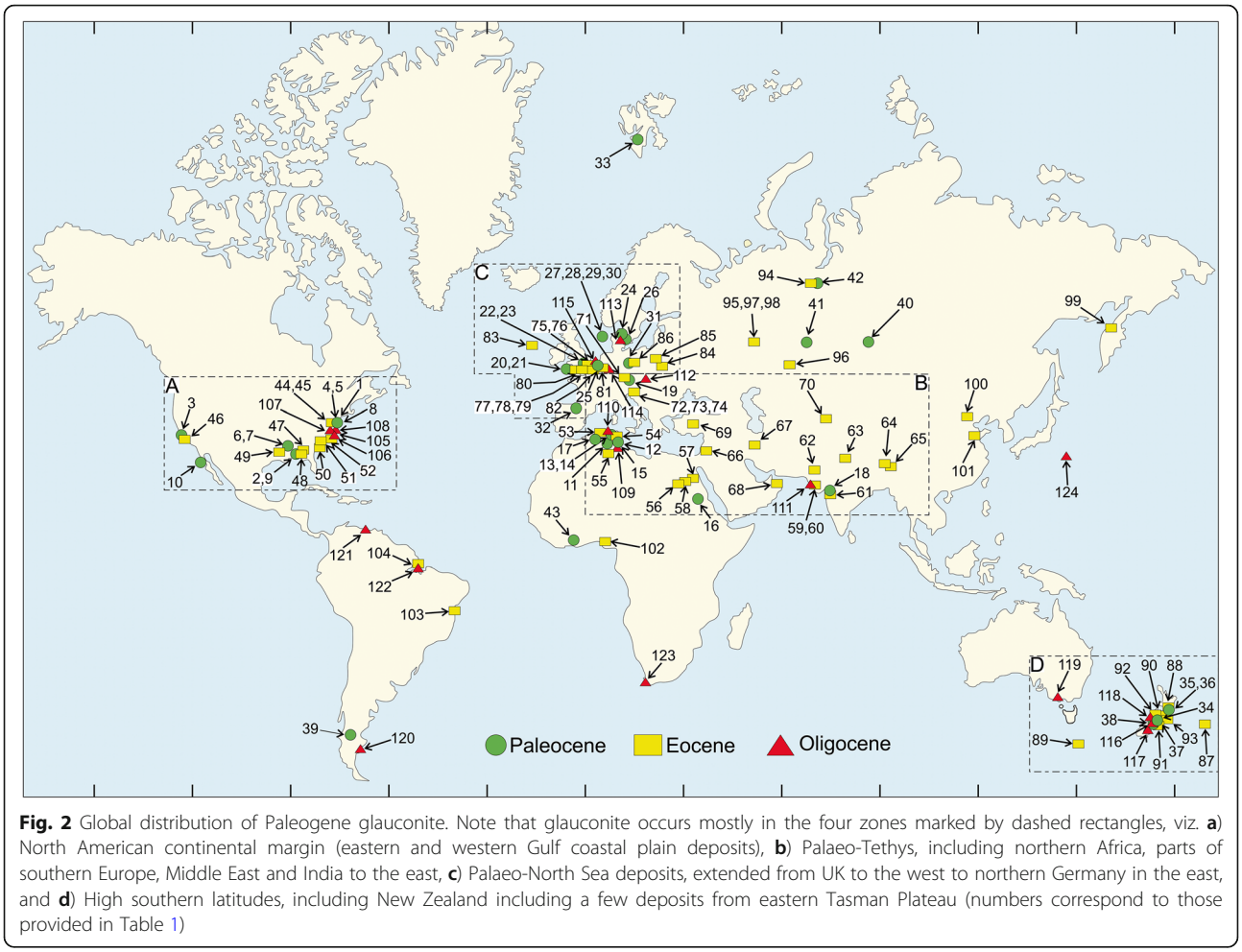

Fig. 2 Global distribution of Paleogene glauconite. Note that glauconite occurs mostly in the four zones marked by dashed rectangles, viz. **a**) North American continental margin (eastern and western Gulf coastal plain deposits), **b**) Palaeo-Tethys, including northern Africa, parts of southern Europe, Middle East and India to the east, **c**) Palaeo-North Sea deposits, extended from UK to the west to northern Germany in the east, and **d**) High southern latitudes, including New Zealand including a few deposits from eastern Tasman Plateau (numbers correspond to those provided in Table 1)

phosphorite deposition shifted towards the eastern and northern parts of the Tethyan domain (Fig. 5). The deposition of phosphorite took place in Iran and in Oman (Beavington-Penney et al. 2006; Zarasvandi et al. 2019) and in Poland (Czuryłowicz et al. 2014). Phosphorite deposition was less common in the Oligocene. Besides the Tethyan margin, glauconite and phosphorite deposits formed within the Oligocene succession of Australia and South Africa (Kelly and Webb 1999; Wigley and Compton 2006; Tóth et al. 2010) (Fig. 6). Throughout the Paleogene, most of the phosphorite–glauconite association was restricted to arid paleoclimate, low-latitudinal passive margin settings (Figs. 3, 4, 5, 6).

3.3 Glauconite–lignite association

Lignite is a common deposit of the Paleogene time (Table 1; Fig. 1). The formation of Paleogene lignite overlaps with glauconite within the warm climatic intervals (Fig. 1). Paleogene glauconite occurs in the same stratigraphic succession with economically exploitable lignite in 15 cases. During the Paleocene, lignites formed within a short span of ~ 10 Ma from late Danian to late Lutetian (Mancini and Tew 1993; Liu et al. 1997; Steurbaut et al. 2003; Egger et al. 2009; Ferrow et al. 2011; Samanta et al. 2013a; Sluijs et al. 2014). The oldest record of the lignite–glauconite association from North American Gulf Coastal Plain deposits corresponds to the Danian–Selandian transition (Fig. 1). At the Paleocene–Eocene transition, lignite formed even at high palaeolatitudes in Svalbard, Norway (Dypvik et al. 2011) (Fig. 3). The late Paleocene and middle Eocene lignite–glauconite associations are best developed in the eastern margin of Tethys (Figs. 3, 4). Lignite formed in restricted marine conditions (Chattoraj et al. 2009; Saraswati et al. 2014, 2018). The glauconite–lignite association reduced abruptly during middle and late Eocene (Fig. 1). During the late Oligocene, lignite–glauconite association was restricted only to palaeo-North Sea basin (De Man and Van Simaeys 2004) (Fig. 5). Lignites formed in humid, tropical to boreotropical, and even warm temperate climatic conditions favoring lush growth of vegetation (Figs. 3, 4, 5, 6). Most lignite–glauconite occurrences of high northern latitudes coincide with the Paleocene–

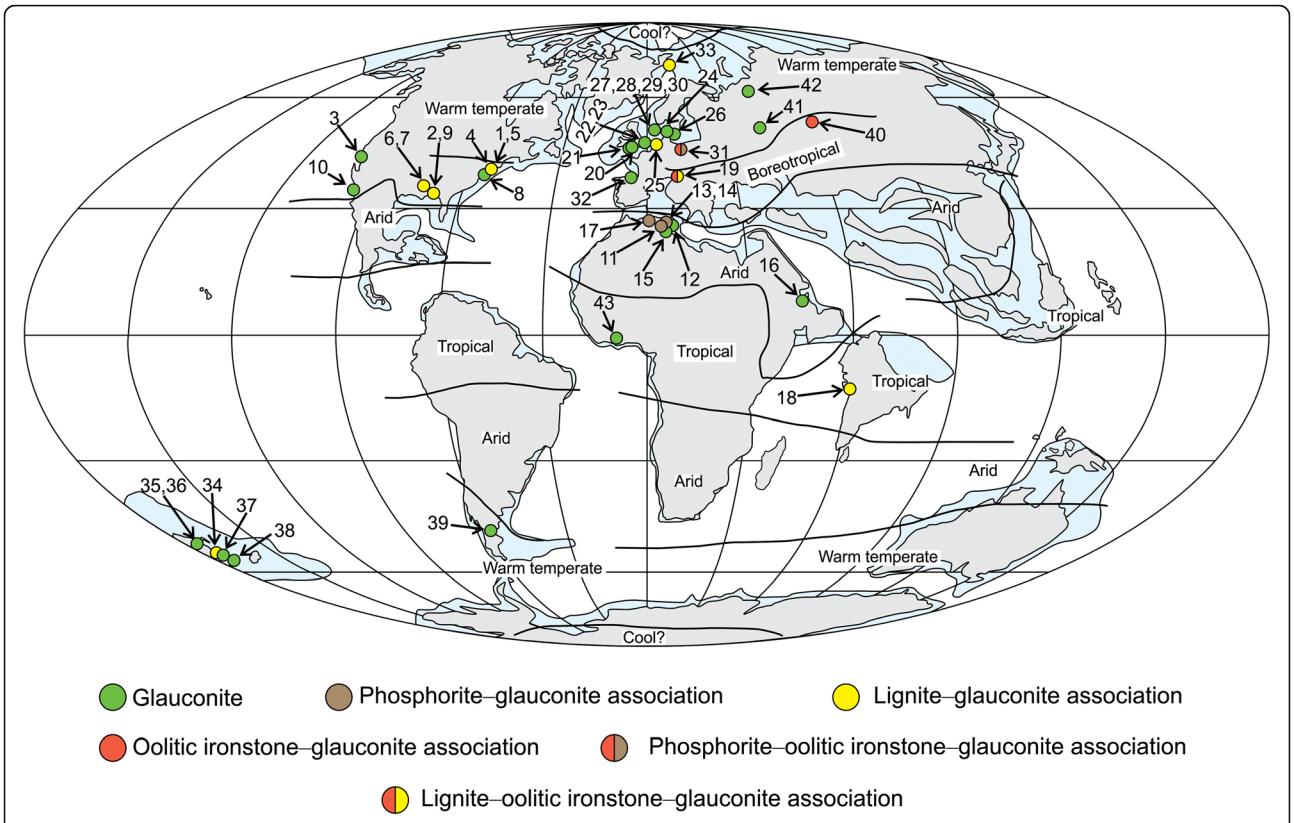

Fig. 3 Palaeogeographic map of Paleocene showing distribution of glauconite–phosphorite, glauconite–lignite and glauconite–oolitic ironstone associations (adapted from Boucot et al. 2013). Note that extensive glauconite–phosphorite association formed along the northern margin of African shelf. Further note that glauconite–lignite association remained confined to tropical climatic zones (numbers correspond to those provided in Table 1)

Eocene transition, but it is restricted to middle Eocene in Russia and late Oligocene in Belgium (Table 1; Figs. 5, 6). At high southern latitude lignite is devoid of glauconite during the Paleocene and early Eocene.

3.4 Glauconite–oolitic ironstone association

Oolitic ironstone deposits contain ~ 5% iron oolith/ooid and more than 15% iron, with goethite, siderite, chamosite, odinite, and berthierine as chief iron-bearing minerals (Rudmin et al. 2019). The majority of the oolitic ironstone of the Cenozoic time preferably formed in the late Paleocene to early–middle Eocene period in marginal marine environments (van Houten 1992; Rudmin et al. 2019). van Houten (1992) found that the majority of the oolitic ironstone deposits of the Cenozoic time are associated with glauconites and phosphorites, hardgrounds and coal measures. Our review reports 14 cases of glauconite–oolitic ironstone association, closely linked to the warming events of the Paleogene (Table 1; Fig. 1). In most of these deposits, glauconite and oolitic ironstone deposited in close proximity to lignite and phosphorite.

Glauconite–oolitic ironstone association occurs within the Paleocene Kressenberg Formation in Austria (Egger et al. 2009) (Fig. 3). Oolitic ironstone deposits proliferate in the London Basin during the late Paleocene and early Eocene (Huggett and Gale 1997). Glauconite–ironstone association declines during the onset of cold climatic conditions after EECO (ca. 50 Ma) (Figs. 1, 5, 6). This deposit in Egypt, Iran, and Oman coincides with middle Eocene climatic optimum (MECO) (Beavington-Penney et al. 2006; Baioumy 2007; El-Habaak et al. 2016; Zarasvandi et al. 2019). The late Oligocene glauconite–oolitic ironstone association occurs in the North American continental shelf deposit, from the palaeo-North Sea basin and high southern latitude deposits in Australia and New Zealand (Kelly and Webb 1999; Hesselbo and Huggett 2001). Oolitic ironstones tend to form in tropical/boreotropical and warm temperate climate during most of the Paleogene. During the middle Eocene, the locus of their formation shifted towards the northern margin of the African Shelf (Fig. 5).

4 Discussion

4.1 The formation of glauconite during warming intervals

Although the allogenic glauconite occasionally occurs in the ancient rock record (Amorosi 1997), the vast

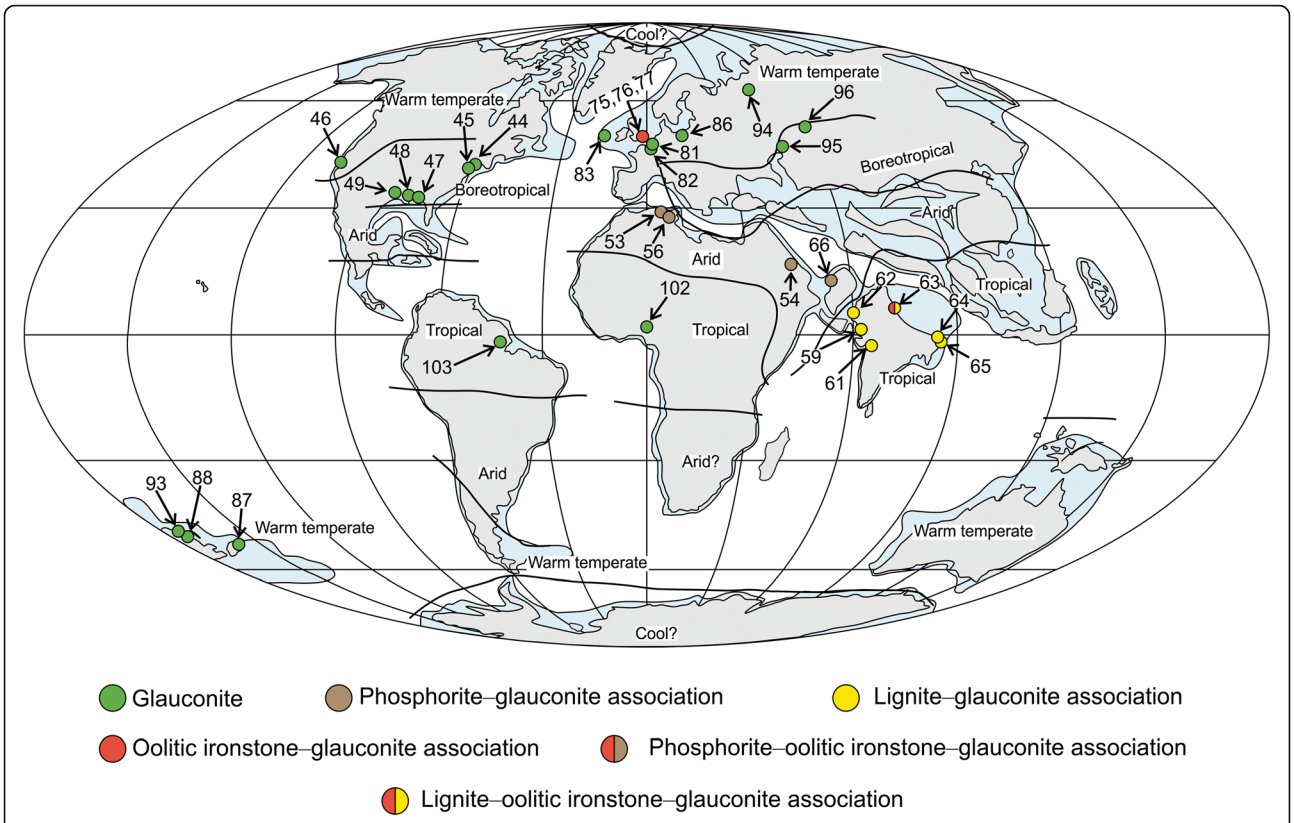

Fig. 4 Palaeogeographic map of early Eocene showing distribution of glauconite–phosphorite, glauconite–lignite and glauconite–oolitic ironstone associations (adapted from Boucot et al. 2013). Note that extensive lignite–glauconite association occurs at the eastern part of Tethys along the Indian subcontinent (numbers correspond to those provided in Table 1)

majority of glauconites form on the seafloor in situ with negligible sediment input (Odin and Matter 1981; El Albani et al. 2005; Amorosi et al. 2007, 2012; Banerjee et al. 2012a, 2012b, 2015, 2016a, 2016b; Baldermann et al. 2013, 2017). Prolonged chemical exchange between seawater and sediments is a prerequisite for the formation of glauconite (Odin and Matter 1981). Several case studies indicate that the composition of glauconite bears subtle evidence of seawater composition of the past (El Albani et al. 2005; Meunier and El Albani 2007; Banerjee et al. 2008, 2015, 2016a, 2016b; Bansal et al. 2017, 2018, 2019, 2020a, 2020b; Tang et al. 2017a, 2017b; Liu et al. 2020; Mandal et al. 2020)

The high global abundance of glauconite in a short time span encompassing the Paleogene warming intervals rules out the local diagenetic effects on the formation of glauconite. Our literature survey shows the distribution of glauconite and other authigenic minerals on the Paleogene ocean floor across the globe. Therefore, the driving factors behind the formation of these authigenic minerals must have acted globally. The close correspondence between the occurrence of glauconite and warming intervals in Paleogene suggests a genetic link between the two (Figs. 1, 7). Several factors determine the formation of glauconite, including depositional conditions, sedimentation rate, seawater temperature, availability of iron and potassium (Odin and Matter 1981; Amorosi 1995, 1997, 2011, 2012; Amorosi and Centineo 1997; El Albani et al. 2005; Amorosi et al. 2007, 2012; Meunier and El Albani 2007; Banerjee et al. 2016a, 2016b; Mandal et al. 2020). The following section discusses the influence of the controlling factors in the formation of authigenic glauconite during the Paleogene.

The depositional environment has strong control over the formation of glauconite by regulating the rate of sedimentation, redox conditions as well as the supply of abundant ions. Although seawater contains abundant potassium, its iron content is very less, particularly in the deep marine environment. Iron is supplied into the shallow sea by the weathering of continental landmasses. However, the depositional environment remains oxic and sediment supply remains high in shallow marine environments, which discourages the growth of glauconite. In modern oceans, glauconite forms abundantly within the outer shelf and deeper environments (Odin and Matter 1981; Amorosi 2012; Banerjee et al. 2016a). However, the Paleogene glauconite formed primarily in

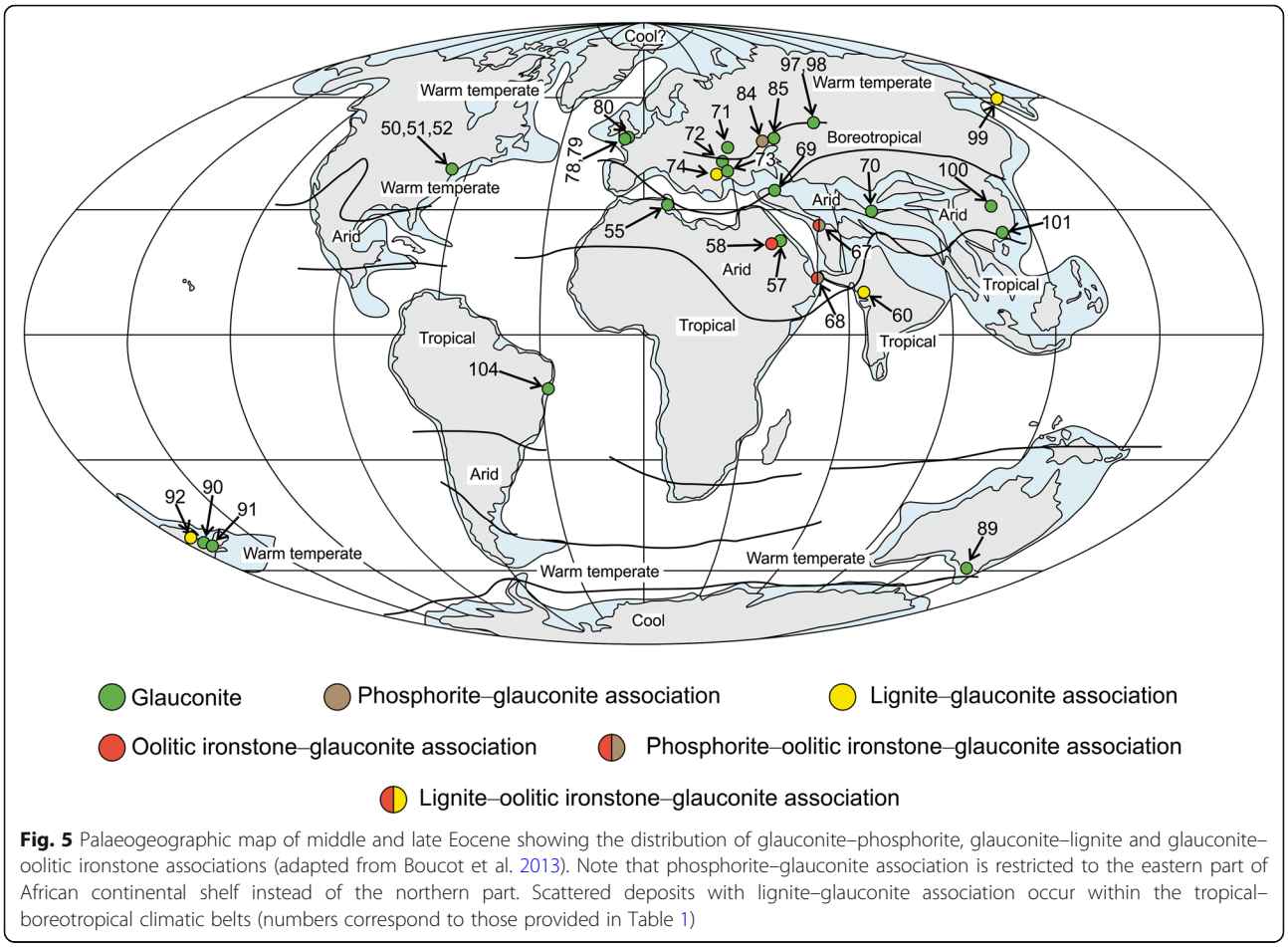

Fig. 5 Palaeogeographic map of middle and late Eocene showing the distribution of glauconite–phosphorite, glauconite–lignite and glauconite–oolitic ironstone associations (adapted from Boucot et al. 2013). Note that phosphorite–glauconite association is restricted to the eastern part of African continental shelf instead of the northern part. Scattered deposits with lignite–glauconite association occur within the tropical–boreotropical climatic belts (numbers correspond to those provided in Table 1)

shallow seas, possibly below the fair-weather wave base (Table 1; Fig. 7). Significantly, glauconites formed predominantly in shallow marine conditions during the Cretaceous period, which is also known for warm climatic conditions (Bansal et al. 2019). However, Bansal et al. (2019) could not establish the relationship between warming intervals and glauconite occurrence because of poor biostratigraphic controls of the Cretaceous successions.

Recent glauconite forms mostly along the eastern and western margins of Africa and North America, southern margin of Australia, and western margin of South America. The formation of glauconite always remained confined within 60° latitudes on both sides of the equator (Porrenga 1968; Odin and Matter 1981). Except for one report of glauconite from Norway, all the Paleogene glauconites also show a similar latitudinal distribution, i.e. within the confinement of 60° palaeo-latitudes. They are absent in the high latitudes (in the Arctic and Antarctic region) (Figs. 3, 4, 5, 6). The absence of glauconite in the polar region and its paucity in the extra-tropical region indicates that a high temperature of seawater facilitates the formation of this mineral. As carbonate deposition shifted to the shallow marine environment during the greenhouse climate, likewise glauconitization too shifted to shallow seas during the Paleogene hyperthermal events. The formation of glauconite is five times slower in the cold water at a depth of 2.5 km, compared to the shallow marine region (Baldermann et al. 2013). Microbiota plays a crucial role in the fixation of iron into the smectite structure, transforming it into glauconite in the modern deep marine environment (Baldermann et al. 2017). In the case of shallow marine glauconite, such a microbial role is not apparent. The chemical composition of deep marine glauconite differs from their shallow marine counterparts by having more Fe_2O_3 and less Al_2O_3 and therefore indicates that the mechanism of formation of this mineral must be different (Baldermann et al. 2017).

The warm and humid climatic conditions during the Paleogene thermal events enhanced the rate of continental weathering (Hessler et al. 2017). Consequently, an increase in the supply of K, Fe, Si, Al, Fe, and Mg ions into the shallow marine environment through riverine input likely to have raised the alkalinity of oceans (Fig. 7). Experimental results indicate that highly alkaline seawater promotes the formation of glauconite (Harder

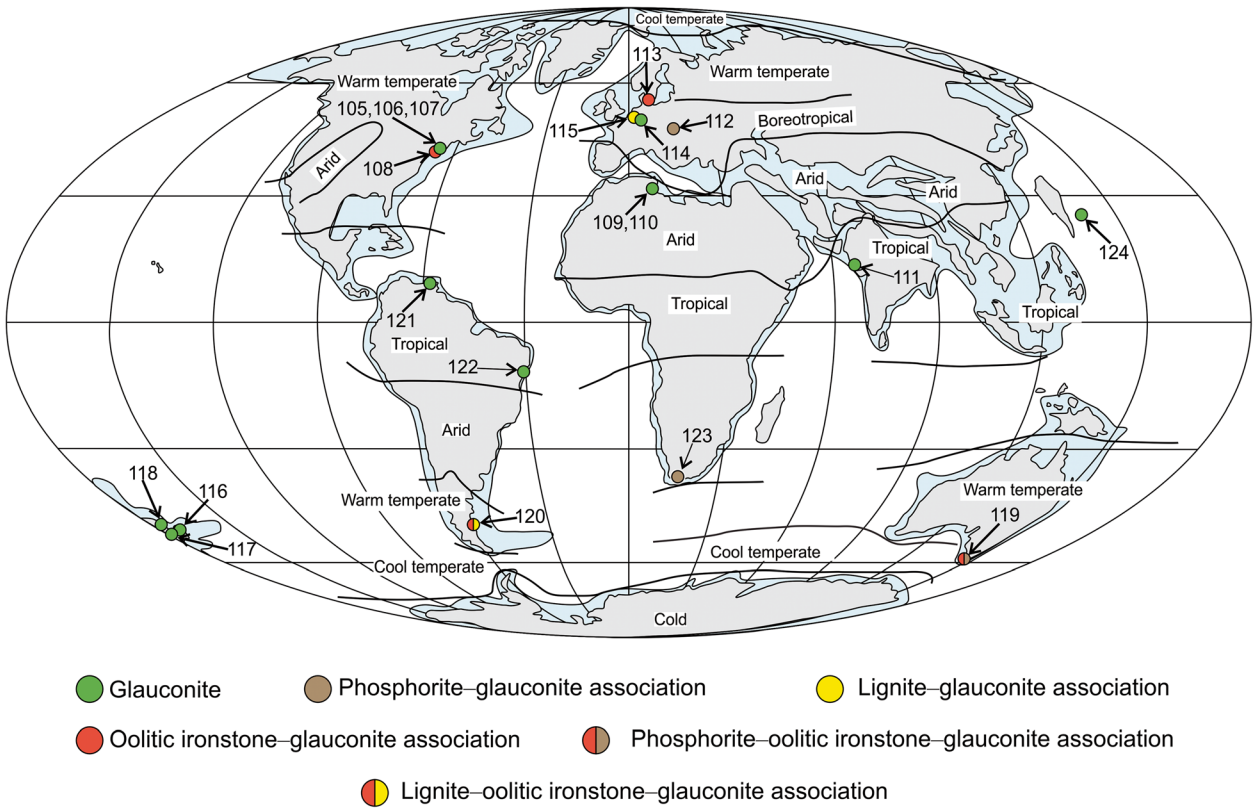

Fig. 6 Palaeogeographic map of Oligocene showing the distribution of glauconite–phosphorite, glauconite–lignite and glauconite–oolitic ironstone associations (adapted from Boucot et al. 2013) (numbers correspond to those provided in Table 1)

1980). Extensive physical reworking of all varieties of continental rocks during the attendant marine transgression further facilitated the release of nutrients to the seawater (Peters and Gaines 2012). The enhanced riverine input during the warm climatic intervals could have provided the required Fe for the formation of glauconite in the shallow marine environment.

The formation of iron-bearing authigenic phases is regulated by the depositional redox condition and the iron reduction reactions (El Albani et al. 2005; Meunier and El Albani 2007; Taylor and Macquaker 2011). Experimental results indicate that sub-oxic condition is a prerequisite for glauconite formation (Harder 1980). Fe occurs as sulfide in reducing conditions in the sulfidic

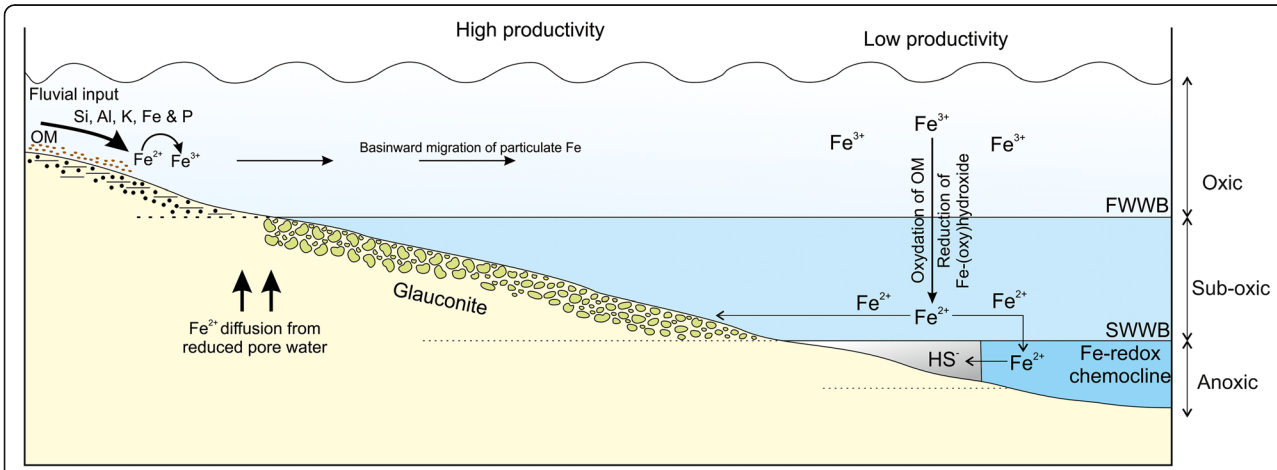

Fig. 7 Model explaining the formation of glauconite in shallow marine environment during the Paleogene time. Phosphorite and ironstone formed broadly in similar conditions. OM: Organic matter; FWWB: Fair-weather wave base; SWWB: Storm-weather wave base

anoxic zone (Berner 1981), while goethite and chamosite forms in oxygenated seawater (Kimberley 1979; Rudmin et al. 2019). However, shallow and intermediate seas presumably became oxygen-deficient during the hyperthermal events (Nicolo et al. 2010; Schulte et al. 2013; Sluijs et al. 2014). The extensive occurrence of Paleogene black shale within the shallow marine Tethyan domain bears testimony to this (Gavrilov et al. 2013; Schulte et al. 2013). Micropalaeontological data of Kutch in India also supports oxygen-deficient shallow marine environments during PETM, ETM2, and ETM3, all of which are characterized by the high abundance of rectilinear benthic foraminifera that is known to be tolerant to low oxygen (Nigam et al. 2007; Khanolkar and Saraswati 2015, 2019). Multiple factors possibly led to this hypoxia on the Paleogene shelves (Fig. 7). The enhanced bioproductivity related to the abundant supply of nutrients created the sub-oxic condition in the shallow marine domain (Sluijs et al. 2014). Widespread hypoxia in marginal marine environments has been documented from Cretaceous global anoxic events (Sluijs et al. 2014). Significant warming during the hyperthermal events led to the discharge of freshwater and nutrients, causing a stratified seawater column and thereby promoting the suboxic to anoxic conditions. Sluggish deep-water circulation further aided the seafloor oxygen depletion (Ridgwell and Schmidt 2010). The glauconite-bearing green shales of Kutch in early and middle Eocene correspond to ETM2 and MECO. These glauconitic shales are typically characterized by tiny, triserial planktic foraminifera *Jenkinsina Columbiana* and *Streptochilus martini* (Kroon and Nederbragt 1990; Kimoto et al. 2009; Khanolkar et al. 2017). Their abundance reaching up to 35% of planktic foraminiferal count suggests high runoff and upwelling conditions in these intervals. Therefore, the availability of abundant continent-derived Fe, as well as the development of the sub-oxic conditions in shallow seas boosted glauconite formation during warm climatic intervals.

A slow rate of sedimentation generally helps the reduced iron to be incorporated into the glauconite structure (Odin and Matter 1981; Meunier and El Albani 2007; Amorosi 2012; Banerjee et al. 2016a, 2016b). The enhanced supply of siliciclastics because of heightened continental weathering during the hyperthermal events should also have raised the sedimentation rate. Although the absolute sea-level rose only about 20 m to 30 m during the hyperthermal events, its rapidness might have led to sediment starvation in shallow seas (Sluijs et al. 2014). The occurrence of around 90% glauconite coinciding with the three warm climatic intervals marked in Fig. 1 indicate that temperature, redox condition of the depositional environment, rapid transgression as well as the availability of abundant nutrients possibly superseded the effect of possible excessive clastic supply into the marine basin related to enhanced weathering during the 'greenhouse world'.

4.2 Factors promoting phosphorite deposition during the Paleogene time

Phosphorite is a common associate of glauconite in the Paleogene (Glenn and Arthur 1990; Kouwenhoven et al. 1997; Kechiched et al. 2018; Metwally and Mahfouz 2018; Banerjee et al. 2019). Conditions favourable for the precipitation of phosphorite and glauconite broadly overlap, requiring depletion in clastic supply and oxygen-depleted seawater. Hypoxic and anoxic bottom seawater facilitates the recycling of phosphorus from organic matter. Sub-oxic Paleogene shelf waters, therefore, remained the favourable sites of formation for both glauconite and phosphorite. Schulte et al. (2013) reported the formation of phosphorite during the recovery phase of the PETM. Phosphorite–glauconite association in modern and ancient sediments forms within a narrow zone lying between upper slope (Fe- and P-poor, TOC enriched) and outer shelf (Fe- and P-enriched), in close vicinity of the oxygen minimum zone (Banerjee et al. 2019 and references therein). Palaeolatitude is also another factor that controls global P-cycle (Soudry et al. 2006). Low latitudes favouring open circulation prefer the accumulation of phosphorite (Cook and McElhinny 1979; Soudry et al. 2006). During most of the Paleogene, the northern part of the African continent remained close to the equator (Figs. 3, 4, 5, 6).

4.3 Factors influencing lignite deposition

Paleogene lignite deposits are predominantly of strand plain origin (Prasad et al. 2013), and they remain confined to the tropical zone along the palaeo-Tethyan margin (Figs. 3, 4, 5, 6; Chattoraj et al. 2009; Egger et al. 2009; Samanta et al. 2013a, 2013b). Lignite deposits form at the top of smaller order shallowing-upward cycles, below the marine flooding surfaces within an overall transgressive deposit (Prasad et al. 2013). Whereas, the occurrence of glauconite coincides with the marine flooding surfaces (Banerjee et al. 2012a, 2012b). A humid climate presumably facilitated the growth of the tropical rainforest during the warmer climatic intervals of Paleogene. Accumulation of abundant vegetal matter in a stagnant marginal marine environment possibly led to lignite formation. Coal deposits during the Paleozoic formed in tropical climates under high rainfall (Cecil et al. 1985). A low rate of clastic input coupled with wet climatic conditions and vegetation cover facilitated coal formation (Cecil 1990). However, glauconite, as well as phosphorite are rarely associated with Paleozoic coal deposits.

Coal/lignite is particularly abundant in several Indian Paleogene basins including Cambay (Prasad et al. 2013; Samanta et al. 2013b), Kutch (Khanolkar and Saraswati 2015 and references therein), Rajasthan (Raju and Mathur 2013) and in Assam-Arakan basin (Saikia et al. 2009). The high abundance of lignite within the Indian Paleogene possibly relates to the formation of a tropical rainforest that leads to the rapid deposition of organic matter and higher land plants into the marginal marine environment (Prasad et al. 2013). Extensive development of marsh-bay complexes characterized the Indian subcontinent that remained close to the equator during the Eocene (Figs. 4, 5) (Prasad et al. 2013).

4.4 Formation of oolitic ironstone during the Paleogene

Glauconite forms an important component within the Paleogene oolitic ironstone deposits along the globe (van Houten 1992). Depositional conditions required for the formation of oolitic ironstone, glauconite, and phosphorite are broadly similar (van Houten 1992; Todd et al. 2019). Although most Paleozoic oolitic ironstones involve upwelling, Cenozoic deposits are controversial in terms of origin. A warm climate and marine transgression favour the formation of oolitic ironstone (Todd et al. 2019). The warm climate facilitates continental weathering and supplies abundant Fe into the shallow marine ocean (see Todd et al. op. cit.). The particulate riverine Fe is trapped mostly in lagoons, estuaries and flood plains before reaching the deep ocean during the rapid transgression (Poulton and Canfield 2011). Further, submarine volcanism, related to ocean floor spreading provides abundant Fe^{2+} into the marine realm. The upwelling current carries additional P^{4+} and Fe^{2+} from the deeper ocean and facilitates the formation of phosphorite, glauconite and oolitic ironstone. Microbial respiration/oxidation of organic matter is further responsible for the formation of anoxic and hypoxic water column in the upwelling front favouring the formation of francolite (and/or pyrite) and Fe-silicates, respectively (Todd et al. 2019). A more oxygenated water column results in the formation of Fe-(oxyhydr)oxide constituting the ironstone facies. Several studies indicated that the formation of oolitic ironstone is favoured immediately after ocean hypoxia (Schulte et al. 2013; Bekker et al. 2014). Therefore, an increase in productivity and related oxygen deficiency provides abundant ferrous iron in shelf waters, thus facilitating massive ironstone deposits during the warm climatic intervals (Homoky 2017; Konhauser et al. 2017). While the pyrite can be formed in hypoxic and anoxic seawater, chamosite and/or berthierine formation is favoured in hypoxic seawater conditions (Berner 1981; Taylor and Macquaker 2011; Todd et al. 2019; Rudmin et al. 2020). Rudmin et al. (op. cit.) established a link between volcanism and oolitic ironstone formation from the Siberian basins. Widespread volcanism in north Atlantic during the early part of Paleogene might have facilitated hypoxic seawater.

5 Conclusions

The review of existing literature establishes a link between Paleogene warming events and authigenic mineralization, with the following conclusions.

1) A review of global occurrences of Paleogene glauconites broadly correspond to warm climatic intervals that witnessed multiple hyperthermal events.
2) The widespread occurrence of glauconite across the globe in the late Paleocene and early Eocene relates to a combination of factors including global sea-level rise, hypoxic shelf, and warm and humid climate. A slow rate of sediment accumulation within the transgressive shallow seas facilitated the formation of glauconite on the seafloor.
3) The depositional conditions of phosphorus and oolitic ironstone are broadly similar to those of glauconite, and therefore, the abundance of these two deposits follows a similar trend.
4) Although the occurrence of authigenic deposits was largely influenced by global climatic conditions, factors like upwelling current and palaeolatitude led to the formation of phosphorite and lignite regionally.
5) Palaeo-latitudinal settings also influenced the occurrence of authigenic deposits. The deposition of phosphorite and lignite deposits was favoured in low palaeolatitudes.
6) Paleogene lignite formed mostly in coastal environments and their formation is facilitated in warm and humid climate. These deposits marked smaller order regressions within an overall transgressive deposit of warm climatic intervals.

Abbreviations

CCD: Calcite compensation depth; CFA: Carbonate fluorapatite; CIE: Carbon isotopic excursion; DAN-C2: Danian C2 event; EECO: Early Eocene climatic optimum; ELMO: Eocene layer of mysterious origin; ELPE: Early late Paleocene event; ETM1: Eocene thermal maximum 1; ETM2: Eocene thermal maximum 2; ETM3: Eocene thermal maximum 3; FO: First occurrence; FWWB: Fair-weather wave base; LDE: Latest Danian event; LO: Last occurrence; LOWE: Late Oligocene warming event; MECO: Middle Eocene climatic optimum; MPBE: Mid Paleocene biotic event; OM: Organic matter; PETM: Paleocene–Eocene thermal maximum; SWWB: Storm-weather wave base

Acknowledgements

Authors acknowledge infrastructure support by Indian Institute of Technology Bombay. Authors thank S.C. Patel and Javed M. Shaikh for providing analytical support to study many glauconite samples over the years at the DST IITB National facility for EPMA, Department of Earth Sciences, Indian Institute of Technology Bombay.

Authors' contributions
SB, TRC and PKS carried out the data analysis and drafted the manuscript. SB conceived the study and helped to revise the manuscript. TRC and SK performed literature survey. PKS took care of biostratigraphic data interpretation. All authors read and approved the final manuscript.

Funding
SB is thankful to Ministry of Mines, Government of India for financial support through grant F No. 14/77/2015- Met. IV. TRC is thankful to Council of Scientific and Industrial Research, India for the financial support.

Availability of data and materials
Since this is a review paper all data analyzed in this study are available in published literature, which are cited in this paper.

Competing interests
The authors declare that they have no competing interests.

Author details
[1]Department of Earth Sciences, Indian Institute of Technology Bombay, Powai, Mumbai 400076, India. [2]Department of Earth Sciences, Indian Institute of Technology Kanpur, Kanpur 208016, India.

Received: 27 April 2020 Accepted: 22 September 2020
Published online: 09 October 2020

References

Aitchison, J.C. 1988. An Eocene storm-generated littoral placer, Northeast Otago. *New Zealand Journal of Geology and Geophysics* 31: 381–383.

Ali, J.R., and D.W. Jolley. 1996. Chronostratigraphic framework for the Thanetian and lower Ypresian deposits of southern England. *Geological Society, London, Special Publications* 101: 129–144.

Amaral, G. 1967. Potassium-argon age measurements on some Brazillian glauconites. *Earth and Planetary Science Letters* 3: 190–192.

Amorosi, A. 1995. Glaucony and sequence stratigraphy; a conceptual framework of distribution in siliciclastic sequences. *Journal of Sedimentary Research* 65: 419–425.

Amorosi, A. 1997. Detecting compositional, spatial, and temporal attributes of glaucony: A tool for provenance research. *Sedimentary Geology* 109: 135–153.

Amorosi, A. 2011. The problem of glaucony from the Shannon sandstone (Campanian, Wyoming). *Terra Nova* 23: 100–107.

Amorosi, A. 2012. The occurrence of glaucony in the stratigraphic record: Distribution patterns and sequence-stratigraphic significance. *International Association of Sedimentologists Special Publications* 45: 37–54.

Amorosi, A., and M.C. Centineo. 1997. Glaucony from the Eocene of the Isle of Wight (southern UK): Implications for basin analysis and sequence-stratigraphic interpretation. *Journal of the Geological Society* 154: 887–896.

Amorosi, A., R. Guidi, R. Mas, and E. Falanga. 2012. Glaucony from the Cretaceous of the sierra de Guadarrama (Central Spain) and its application in a sequence-stratigraphic context. *International Journal of Earth Sciences* 101: 415–427.

Amorosi, A., I. Sammartino, and F. Tateo. 2007. Evolution patterns of glaucony maturity: A mineralogical and geochemical approach. *Deep Sea Research Part II: Topical Studies in Oceanography* 54: 1364–1374.

Aubry, M.P. 1985. Northwestern European Paleogene magnetostratigraphy, biostratigraphy, and paleogeography: Calcareous nannofossil evidence. *Geology* 13: 198–202.

Ayress, M.A. 2006. Ostracod biostratigraphy of the Oligocene-Miocene (upper Waitakian to lower Otaian) in southern New Zealand. *New Zealand Journal of Geology and Geophysics* 49: 359–373.

Baioumy, H.M. 2007. Iron–phosphorus relationship in the iron and phosphorite ores of Egypt. *Geochemistry* 67: 229–239.

Baldermann, A., M. Dietzel, V. Mavromatis, F. Mittermayr, L.N. Warr, and K. Wemmer. 2017. The role of Fe on the formation and diagenesis of interstratified glauconite-smectite and illite-smectite: A case study of Upper Cretaceous shallow-water carbonates. *Chemical Geology* 453: 21–34.

Baldermann, A., L.N. Warr, G.H. Grathoff, and M. Dietzel. 2013. The rate and mechanism of deep-sea glauconite formation at the Ivory Coast–Ghana marginal ridge. *Clays and Clay Minerals* 61: 258–276.

Banerjee, S., U. Bansal, K. Pande, and S.S. Meena. 2016b. Compositional variability of glauconites within the Upper Cretaceous Karai Shale Formation, Cauvery Basin, India: Implications for evaluation of stratigraphic condensation. *Sedimentary Geology* 331: 12–29.

Banerjee, S., U. Bansal, and A.V. Thorat. 2016a. A review on palaeogeographic implications and temporal variation in glaucony composition. *Journal of Palaeogeography* 5 (1): 43–71.

Banerjee, S., S.L. Chattoraj, P.K. Saraswati, S. Dasgupta, and U. Sarkar. 2012b. Substrate control on formation and maturation of glauconites in the middle Eocene Harudi formation, western Kutch, India. *Marine and Petroleum Geology* 30: 144–160.

Banerjee, S., S.L. Chattoraj, P.K. Saraswati, S. Dasgupta, U. Sarkar, and A. Bumby. 2012a. The origin and maturation of lagoonal glauconites: A case study from the Oligocene Maniyara fort formation, western Kutch, India. *Geological Journal* 47: 357–371.

Banerjee, S., S. Farouk, E. Nagm, T.R. Choudhury, and S.S. Meena. 2019. High mg-glauconite in the Campanian Duwi formation of Abu Tartur plateau, Egypt and its implications. *Journal of African Earth Sciences* 156: 12–25.

Banerjee, S., S. Jeevankumar, and P.G. Eriksson. 2008. Mg-rich ferric illite in marine transgressive and highstand systems tracts: Examples from the Paleoproterozoic Semri group, Central India. *Precambrian Research* 162: 212–226.

Banerjee, S., S. Mondal, P.P. Chakraborty, and S.S. Meena. 2015. Distinctive compositional characteristics and evolutionary trend of Precambrian glaucony: Example from Bhalukona formation, Chhattisgarh basin, India. *Precambrian Research* 271: 33–48.

Bansal, U., S. Banerjee, and R. Nagendra. 2020b. Is the rarity of glauconite in Precambrian deposits related to its transformation to chlorite? *Precambrian Research*: 336. https://doi.org/10.1016/j.precamres.2019.105509.

Bansal, U., S. Banerjee, K. Pande, A. Arora, and S.S. Meena. 2017. The distinctive compositional evolution of glauconite in the Cretaceous Ukra Hill Member (Kutch Basin, India) and its implications. *Marine and Petroleum Geology* 82: 97–117.

Bansal, U., S. Banerjee, K. Pande, and D.K. Ruidas. 2020a. Unusual seawater composition of the Late Cretaceous Tethys imprinted in glauconite of Narmada Basin, central India. *Geological Magazine* 157: 233–247.

Bansal, U., S. Banerjee, D.K. Ruidas, and K. Pande. 2018. Origin and geochemical characterization of the glauconites in the Upper Cretaceous Lameta Formation, central India. *Journal of Palaeogeography* 7 (1): 99–116.

Bansal, U., K. Pande, S. Banerjee, R. Nagendra, and K.C. Jagadeesan. 2019. The timing of oceanic anoxic events in the Cretaceous succession of Cauvery Basin: Constraints from $^{40}Ar/^{39}Ar$ ages of glauconite in the Karai Shale Formation. *Geological Journal* 54: 308–315.

Beavington-Penney, S.J., V.P. Wright, and A. Racey. 2006. The middle Eocene Seeb formation of Oman: An investigation of acyclicity, stratigraphic completeness, and accumulation rates in shallow marine carbonate settings. *Journal of Sedimentary Research* 76: 1137–1161.

Bekker, A., N. Planavsky, B. Rasmussen, B. Krapez, A. Hofmann, J. Slack, O. Rouxel, and K. Konhauser. 2014. Iron formations: Their origins and implications for ancient seawater chemistry. In *Treatise on geochemistry*, ed. H. Holland and K. Turekian, 561–628. Amsterdam: Elsevier. https://doi.org/10.1016/B978-0-08-095975-7.00719-1.

Bektemirova, T., A. Bakirov, R. Hu, H. He, Y. Cai, W. Tan, and A. Chen. 2018. Mineralogical evolution of the Paleogene formations in the Kyzyltokoy Basin, Kyrgyzstan: Implications for the formation of glauconite. *Clays and Clay Minerals* 66: 43–60.

Bernaola, G., J.I. Baceta, X. Orue-Etxebarria, L. Alegret, M. Martin-Rubio, J. Arostegui, and J. Dinarès-Turell. 2007. Evidence of an abrupt environmental disruption during the mid-Paleocene biotic event (Zumaia section, western Pyrenees). *Geological Society of America Bulletin* 119: 785–795.

Berner, R.A. 1981. A new geochemical classification of sedimentary environments. *Journal of Sedimentary Research* 51: 359–365.

Bornemann, A., P. Schulte, J. Sprong, E. Steurbaut, M.A. Youssef, and R.P. Speijer. 2009. Latest Danian carbon isotope anomaly and associated environmental change in the southern Tethys (Nile Basin, Egypt). *Journal of the Geological Society of London* 166: 1135–1142.

Bosboom, R., O. Mandic, G. Dupont-Nivet, J.N. Proust, C. Ormukov, and J. Aminov. 2017. Late Eocene palaeogeography of the proto-Paratethys Sea in Central Asia (NW China, southern Kyrgyzstan and SW Tajikistan). *Geological Society, London, Special Publications* 427: 565–588.

Boucot, A.J., C. Xu, C.R. Scotese, and R.J. Morley. 2013. *Phanerozoic Paleoclimate: An Atlas of Lithologic Indicators of Climate*, SEPM Concepts in Sedimentology and Paleontology 11, 478. Tulsa: Society for Sedimentary Geology.

Boukhalfa, K., A. Amorosi, M. Soussi, and K.B. Ismail-Lattrâche. 2015. Glauconitic-rich strata from Oligo-Miocene shallow-marine siliciclastic deposits of the northern margin of Africa (Tunisia): Geochemical approach for basin analysis. *Arabian Journal of Geosciences* 8: 1731–1742.

Boukhalfa, K., M. Soussi, E. Ozcan, S. Banerjee, and A. Tounekti. 2020. The Oligo-Miocene siliciclastic foreland basin deposits of northern Tunisia: Stratigraphy, sedimentology and paleogeography. *Journal of African Earth Sciences*. https://doi.org/10.1016/j.jafrearsci.2020.103932.

Bralower, T.J., I. Premoli Silva, and M.J. Malone. 2002. New evidence for abrupt climate change in the Cretaceous and Paleogene: An ocean drilling program expedition to Shatsky rise, Northwest Pacific. *Geological Society of America Today* 12: 4–10.

Burst, J.F. 1958. "Glauconite" pellets: Their mineral nature and applications to stratigraphic interpretations. *AAPG Bulletin* 42: 310–327.

Campbell, H.J., P.B. Andrews, A.G. Beu, A.R. Edwards, N.D. Hornibrook, M.G. Laird, P.A. Maxwell, and W.A. Watters. 1988. Cretaceous–Cenozoic lithostratigraphy of the Chatham Islands. *Journal of the Royal Society of New Zealand* 18: 285–308.

Cecil, C.B. 1990. Paleoclimate controls on stratigraphic repetition of chemical and siliciclastic rocks. *Geology* 18: 533–536.

Cecil, C.B., R.W. Stanton, S.G. Neuzil, F.T. Dulong, L.F. Ruppert, and B.S. Pierce. 1985. Paleoclimate controls on late Paleozoic sedimentation and peat formation in the central Appalachian Basin (USA). *International Journal of Coal Geology* 5: 195–230.

Chattoraj, S.L., S. Banerjee, and P.K. Saraswati. 2009. Glauconites from the late Palaeocene–early Eocene Naredi formation, western Kutch and their genetic implications. *Journal of the Geological Society of India* 73: 567.

Clark, M., and A. Robertson. 2005. Uppermost Cretaceous–lower Tertiary Ulukışla Basin, south-central Turkey: Sedimentary evolution of part of a unified basin complex within an evolving Neotethyan suture zone. *Sedimentary Geology* 173: 15–51.

Clemmensen, A., and E. Thomsen. 2005. Palaeoenvironmental changes across the Danian–Selandian boundary in the North Sea Basin. *Palaeogeography, Palaeoclimatology, Palaeoecology* 219: 351–394.

Cook, P.J., and M.W. McElhinny. 1979. A reevaluation of the spatial and temporal distribution of sedimentary phosphate deposits in the light of plate tectonics. *Economic Geology* 74: 315–330.

Cosović, V., and K. Drobne. 1995. Palaeoecological significance of morphology of orthophragminids from the Istrian peninsula (Croatia and Slovenia). *Geobios* 28: 93–99.

Cosović, V., K. Drobne, and A. Moro. 2004. Paleoenvironmental model for Eocene foraminiferal limestones of the Adriatic carbonate platform (Istrian peninsula). *Facies* 50: 61–75.

Cramer, B.S., M.P. Aubry, K.G. Miller, R.K. Olsson, J.D. Wright, and D.V. Kent. 1999. An exceptional chronologic, isotopic, and clay mineralogic record of the latest Paleocene thermal maximum, Bass River, NJ, ODP 174AX. *Bulletin de la Société géologique de France* 170: 883–897.

Cramer, B.S., J.D. Wright, D.V. Kent, and M.P. Aubry. 2003. Orbital climate forcing of $\delta^{13}C$ excursions in the late Paleocene–early Eocene (chrons C24n–C25n). *Paleoceanography* 18 (4). https://doi.org/10.1029/2003PA000909.

Crouch, E.M., G.R. Dickens, H. Brinkhuis, M.P. Aubry, C.J. Hollis, K.M. Rogers, and H. Visscher. 2003. The Apectodinium acme and terrestrial discharge during the Paleocene–Eocene thermal maximum: New palynological, geochemical and calcareous nannoplankton observations at Tawanui, New Zealand. *Palaeogeography, Palaeoclimatology, Palaeoecology* 194: 387–403.

Crouch, E.M., C. Heilmann-Clausen, H. Brinkhuis, H.E. Morgans, K.M. Rogers, H. Egger, and B. Schmitz. 2001. Global dinoflagellate event associated with the late Paleocene thermal maximum. *Geology* 29: 315–318.

Czuryłowicz, K., A. Lejzerowicz, S. Kowalczyk, and A. Wysocka. 2014. The origin and depositional architecture of Paleogene quartz-glauconite sands in the Lubartów area, eastern Poland. *Geological Quarterly* 58: 125–144.

Dallanave, E., V. Bachtadse, E.M. Crouch, L. Tauxe, C.L. Shepherd, H.E. Morgans, C.J. Hollis, B.R. Hines, and S. Sugisaki. 2016. Constraining early to middle Eocene climate evolution of the Southwest Pacific and Southern Ocean. *Earth and Planetary Science Letters* 433: 380–392.

De Man, E., and S. Van Simaeys. 2004. Late Oligocene warming event in the southern North Sea Basin: Benthic foraminifera as paleotemperature proxies. *Netherlands Journal of Geosciences* 83: 227–239.

Dill, H.G., A. Köthe, F. Gramann, and R. Botz. 1996. A palaeoenvironmental and palaeoecological analysis of fine-grained Paleogene estuarine deposits of North Germany. *Palaeogeography, Palaeoclimatology, Palaeoecology* 124: 273–326.

Dix, G.R., and A. Parras. 2014. Integrated diagenetic and sequence stratigraphy of a late Oligocene–early Miocene, mixed-sediment platform (Austral Basin, southern Patagonia): Resolving base-level and paleoceanographic changes, and paleoaquifer characteristics. *Sedimentary Geology* 307: 17–33.

Duarte, M.A.T., and M.L. Martínez. 2002. K–Ar dating and geological significance of clastic sediments of the Paleocene Sepultura formation, Baja California, México. *Journal of South American Earth Sciences* 15: 725–730.

Dypvik, H., L. Riber, F. Burca, D. Rüther, D. Jargvoll, J. Nagy, and M. Jochmann. 2011. The Paleocene–Eocene thermal maximum (PETM) in Svalbard — Clay mineral and geochemical signals. *Palaeogeography, Palaeoclimatology, Palaeoecology* 302: 156–169.

Egger, H., C. Heilmann-Clausen, and B. Schmitz. 2009. From shelf to abyss: Record of the Paleocene/Eocene-boundary in the eastern Alps (Austria). *Geologica Acta: an International Earth Science Journal* 7: 215–227.

El Albani, A., A. Meunier, and F. Fürsich. 2005. Unusual occurrence of glauconite in a shallow lagoonal environment (Lower Cretaceous, northern Aquitaine Basin, SW France). *Terra Nova* 17: 537–544.

El-Habaak, G., M. Askalany, M. Galal, and M. Abdel-Hakeem. 2016. Upper Eocene glauconites from the Bahariya depression: An evidence for the marine regression in Egypt. *Journal of African Earth Sciences* 117: 1–11.

Ellison, R.A., J.R. Ali, N.M. Hine, and D.W. Jolley. 1996. Recognition of chron C25n in the upper Paleocene Upnor formation of the London Basin, UK. *Geological Society, London, Special Publications* 101: 185–193.

Ferrow, E., V. Vajda, C.B. Koch, B. Peucker-Ehrenbrink, and P.S. Willumsen. 2011. Multiproxy analysis of a new terrestrial and a marine Cretaceous–Paleogene (K–Pg) boundary site from New Zealand. *Geochimica et Cosmochimica Acta* 75: 657–672.

Fitch, F.J., P.J. Hooker, J.A. Miller, and N.R. Brereton. 1978. Glauconite dating of Palaeocene-Eocene rocks from East Kent and the time-scale of Palaeogene volcanism in the North Atlantic region. *Journal of the Geological Society* 135: 499–512.

Franzosi, C., L.N. Castro, and A.M. Celeda. 2014. Technical evaluation of glauconies as alternative potassium fertilizer from the Salamanca formation, Patagonia, Southwest Argentina. *Natural Resources Research* 23: 311–320.

Frieling, J., A.I. Iakovleva, G.J. Reichart, G.N. Aleksandrova, Z.N. Gnibidenko, S. Schouten, and A. Sluijs. 2014. Paleocene–Eocene warming and biotic response in the epicontinental west Siberian Sea. *Geology* 42: 767–770.

Garnit, H., S. Bouhlel, and I. Jarvis. 2017. Geochemistry and depositional environments of Paleocene–Eocene phosphorites: Metlaoui group, Tunisia. *Journal of African Earth Sciences* 134: 704–736.

Gavrilov, Y.O., E.A. Shcherbinina, O.V. Golovanova, and B.G. Pokrovskii. 2013. The late Cenomanian paleoecological event (OAE 2) in the eastern Caucasus basin of northern Peri-Tethys. *Lithology and Mineral Resources* 48: 457–488.

Gedl, P. 2014. Eocene dinoflagellate cysts from the Sołokija Graben (Roztocze, SE Poland). *Geological Quarterly* 58: 707–728.

Geptner, A.R., T.A. Ivanovskaya, E.V. Pokrovskaya, and N.P. Kuralenko. 2008. Glauconite from Paleogene volcano-terrigenous rocks in Western Kamchatka. *Lithology and Mineral Resources* 43: 228–249.

Gibson, T.G., L.M. Bybell, and D.B. Mason. 2000. Stratigraphic and climatic implications of clay mineral changes around the Paleocene/Eocene boundary of the northeastern US margin. *Sedimentary Geology* 134: 65–92.

Gibson, T.G., L.M. Bybell, and J.P. Owens. 1993. Latest Paleocene lithologic and biotic events in neritic deposits of southwestern New Jersey. *Paleoceanography* 8: 495–514.

Glenn, C.R., and M.A. Arthur. 1990. Anatomy and origin of a Cretaceous phosphorite-greensand giant, Egypt. *Sedimentology* 37: 123–154.

Goodman, D.K. 1979. Dinoflagellate "communities"; from the lower Eocene Nanjemoy formation of Maryland USA. *Palynology* 3: 169–190.

Gradstein, F.M., J.G. Ogg, M.B. Schmitz, and G.M. Ogg. 2012. *The Geologic Time Scale 2012*. Elsevier, Amsterdam.

Hamberg, L., G. Dam, C. Wilhelmson, and T.G. Ottesen. 2005. Paleocene deep-marine sandstone plays in the Siri canyon, offshore Denmark–southern Norway. In Geological Society, London, Petroleum Geology Conference Series, eds. A.G. Doré, and B.A. Vining. 6: 1185–1198. Geological Society of London.

Haq, B.U., J. Hardenbol, and P.R. Vail. 1987. Chronology of fluctuating sea levels since the Triassic. *Science* 235: 1156–1167.

Harder, H. 1980. Syntheses of glauconite at surface temperatures. *Clays and Clay Minerals* 28: 217–222.

Harland, W.B., A.V. Cox, P.G. Llewellyn, C.A.G. Pickton, A.G. Smith, and R. Walters. 1982. *A Geologic Time Scale*. Cambridge: Cambridge University Press.

Harris, W.B., P.D. Fullagar, and J.A. Winters. 1984. Rb–Sr glauconite ages, Sabinian, Claibornian and Jacksonian units, southeastern Atlantic coastal plain, USA. *Palaeogeography, Palaeoclimatology, Palaeoecology* 47: 53–76.

Hegab, O.A., and A.G.A. El-Wahed. 2016. Origin of the glauconite from the middle Eocene, Qarara formation, Egypt. *Journal of African Earth Sciences* 123: 21–28.

Hesselbo, S.P., and J.M. Huggett. 2001. Glaucony in ocean-margin sequence stratigraphy (Oligocene–Pliocene, offshore New Jersey, USA; ODP leg 174A). *Journal of Sedimentary Research* 71: 599–607.

Hessler, A.M., J. Zhang, J. Covault, and W. Ambrose. 2017. Continental weathering coupled to Paleogene climate changes in North America. *Geology* 45: 911–914.

Hines, B.R., D.K. Kulhanek, C.J. Hollis, C.B. Atkins, and H.E.G. Morgans. 2013. Paleocene–Eocene stratigraphy and paleoenvironment at Tora, Southeast Wairarapa, New Zealand. *New Zealand Journal of Geology and Geophysics* 56: 243–262.

Homoky, W.B. 2017. Biogeochemistry: Deep ocean iron balance. *Nature Geoscience* 10: 162–163.

Hower, J. 1961. Some factors concerning the nature and origin of glauconite. *American Mineralogist* 46: 313–334.

Huggett, J., J. Adetunji, F. Longstaffe, and D. Wray. 2017. Mineralogical and geochemical characterisation of warm-water, shallow-marine glaucony from the tertiary of the London Basin. *Clay Minerals* 52: 25–50.

Huggett, J.M., and J. Cuadros. 2010. Glauconite formation in lacustrine/palaeosol sediments, Isle of Wight (Hampshire Basin), UK. *Clay Minerals* 45: 35–49.

Huggett, J.M., and A.S. Gale. 1997. Petrology and palaeoenvironmental significance of glaucony in the Eocene succession at Whitecliff Bay, Hampshire Basin, UK. *Journal of the Geological Society* 154: 897–912.

Hughes, A.D., and D. Whitehead. 1987. Glauconitization of detrital silica substrates in the Barton formation (upper Eocene) of the Hampshire Basin, southern England. *Sedimentology* 34: 825–835.

Iakovleva, A.I., and I.A. Kulkova. 2003. Paleocene–Eocene dinoflagellate zonation of Western Siberia. *Review of Palaeobotany and Palynology* 123: 185–197.

Jenkyns, H.C. 2003. Evidence for rapid climate change in the Mesozoic–Palaeogene greenhouse world. *Philosophical Transactions of the Royal Society of London. Series A: Mathematical, Physical and Engineering Sciences* 361: 1885–1916.

Jiang, Z., D. Chen, L. Qiu, H. Liang, and J. Ma. 2007. Source-controlled carbonates in a small Eocene half-graben lake basin (Shulu sag) in Central Hebei Province, North China. *Sedimentology* 54: 265–292.

John, C.M., S.M. Bohaty, J.C. Zachos, A. Sluijs, S. Gibbs, H. Brinkhuis, and T.J. Bralower. 2008. North American continental margin records of the Paleocene–Eocene thermal maximum: Implications for global carbon and hydrological cycling. *Paleoceanography* 23. https://doi.org/10.1029/2007PA001465.

Jorry, S., E. Davaud, and B. Caline. 2003. Controls on the distribution of nummulite facies: A case study from the late Ypresian El Garia formation (Kesra plateau, Central Tunisia). *Journal of Petroleum Geology* 26: 283–306.

Kalia, P., and R. Kintso. 2006. Planktonic foraminifera at the Paleocene/Eocene boundary in the Jaisalmer Basin, Rajasthan, India. *Micropaleontology* 52: 521–536.

Kechiched, R., R. Laouar, O. Bruguier, S. Salmi-Laouar, L. Kocsis, D. Bosch, A. Foufou, O. Ameur-Zaimeche, and H. Larit. 2018. Glauconite-bearing sedimentary phosphorites from the Tébessa region (eastern Algeria): Evidence of REE enrichment and geochemical constraints on their origin. *Journal of African Earth Sciences* 145: 190–200.

Kelly, D.C. 2002. Response of Antarctic (ODP site 690) planktonic foraminifera to the Paleocene–Eocene thermal maximum: Faunal evidence for ocean/climate change. *Paleoceanography* 17 (4): 1071. https://doi.org/10.1029/2002PA000761.

Kelly, J.C., and J.A. Webb. 1999. The genesis of glaucony in the Oligo–Miocene Torquay group, southeastern Australia: Petrographic and geochemical evidence. *Sedimentary Geology* 125: 99–114.

Khanolkar, S., and P.K. Saraswati. 2015. Ecological response of shallow-marine foraminifera to early Eocene warming in equatorial India. *The Journal of Foraminiferal Research* 45: 293–304.

Khanolkar, S., and P.K. Saraswati. 2019. Eocene foraminiferal biofacies in Kutch Basin (India) in context of palaeoclimate and palaeoecology. *Journal of Palaeogeography* 8 (1): 1–16.

Khanolkar, S., P.K. Saraswati, and K. Rogers. 2017. Ecology of foraminifera during the middle Eocene climatic optimum in Kutch, India. *Geodinamica Acta* 29: 181–193.

Kharkwal, A.D. 1966. Glauconite in the Subathu beds (Eocene) of the Simla Hills of India. *Nature* 211: 615.

Kimberley, M.M. 1979. Origin of oolitic iron formations. *Journal of Sedimentary Research* 49: 111–131.

Kimoto, K., T. Ishimura, U. Tsunogai, T. Itaki, and Y. Ujiié. 2009. The living triserial planktic foraminifer Gallitellia vivans (Cushman): Distribution, stable isotopes, and paleoecological implications. *Marine Micropaleontology* 71: 71–79.

Knox, R.W.B. 1979. Igneous grains associated with zeolites in the Thanet beds of Pegwell Bay, Northeast Kent. *Proceedings of the Geologists' Association* 90: 55–59.

Konhauser, K.O., N.J. Planavsky, D.S. Hardisty, L.J. Robbins, T.J. Warchola, R. Haugaard, S.V. Lalonde, C.A. Partin, P.B.H. Oonk, H. Tsikos, and T.W. Lyons. 2017. Iron formations: A global record of Neoarchaean to Palaeoproterozoic environmental history. *Earth-Science Reviews* 172: 140–177.

Kouwenhoven, T.J., R.P. Speijer, C.W.M. Van Oosterhout, and G.J. Van der Zwaan. 1997. Benthic foraminiferal assemblages between two major extinction events: The Paleocene El kef section, Tunisia. *Marine Micropalaentology* 29: 105–127.

Kroon, D., and A.J. Nederbragt. 1990. Ecology and paleoecology of triserial planktic foraminifera. *Marine Micropalaentology* 16: 25–38.

Lewis, D.W., and S. Belliss. 1984. Mid tertiary unconformities in the Waitaki subdivision, North Otago. *Journal of the Royal Society of New Zealand* 14: 251–276.

Li, Q., P.J. Davies, and B. McGowran. 1999. Foraminiferal sequence biostratigraphy of the Oligo-Miocene Janjukian strata from Torquay, southeastern Australia. *Australian Journal of Earth Sciences* 46: 261–273.

Liu, A., D. Tang, X. Shi, X. Zhou, L. Zhoue, M. Shang, Y. Li, and H. Fang. 2020. Mesoproterozoic oxygenated deep seawater recorded by early

diagenetic carbonate concretions from the member IV of the Xiamaling formation, North China. *Precambrian Research* 341: 105667.

Liu, C., J.V. Browning, K.G. Miller, and R.K. Olsson. 1997. Upper Cretaceous to Miocene planktonic foraminiferal biostratigraphy: Results of leg 150X, the New Jersey coastal plain drilling project. In *Proceedings of the Ocean Drilling Program. Scientific Results*, ed. K.G. Miller and S.W. Snyder, vol. 156, 111–127.

Lourens, L.J., A. Sluijs, D. Kroon, J.C. Zachos, E. Thomas, U. Röhl, J. Bowles, and I. Raffi. 2005. Astronomical pacing of late Palaeocene to early Eocene global warming events. *Nature* 435: 1083–1087.

Lucas, J., and L. Prévôt-Lucas. 1995. Tethyan phosphates and bioproductites. In *The Tethys Ocean*, ed. A.E.M. Nairn, L.E. Ricou, B. Vrielynck, and J. Dercourt, 367–391. Boston: Springer.

Lurcock, P.C., and G.S. Wilson. 2013. The palaeomagnetism of glauconitic sediments. *Global and Planetary Change* 110: 278–288.

MacGregor, A.R. 1983. The Waitakere limestone, a temperate algal carbonate in the lower tertiary of New Zealand. *Journal of the Geological Society* 140: 387–399.

Mancini, E.A. 1981. Lithostratigraphy and biostratigraphy of Paleocene subsurface strata in Southwest Alabama. *Gulf Coast Association of Geological Societies Transactions* 31: 359–367.

Mancini, E.A., and B.H. Tew. 1993. Eustasy versus subsidence: Lower Paleocene depositional sequences from southern Alabama, eastern gulf coastal plain. *Geological Society of America Bulletin* 105: 3–17.

Mandal, S., S. Banerjee, S. Sarkar, I. Mondal, and T.R. Choudhury. 2020. Origin and sequence stratigraphic implications of high-alumina glauconite within the lower quartzite, Vindhyan Supergroup. *Marine and Petroleum Geology* 112. https://doi.org/10.1016/j.marpetgeo.2019.104040.

Marivaux, L., E.M. Essid, W. Marzougui, H. Khayati Ammar, S. Adnet, B. Marandat, G. Merzeraud, A. Ramdarshan, R. Tabuce, M. Vianey-Liaud, and J. Yans. 2014. A morphological intermediate between eosimiiform and simiiform primates from the late middle Eocene of Tunisia: Macroevolutionary and paleobiogeographic implications of early anthropoids. *American Journal of Physical Anthropology* 154: 387–401.

McConchie, D.M., and D.W. Lewis. 1978. Authigenic, perigenic, and allogenic glauconites from the Castle Hill basin, North Canterbury, New Zealand. *New Zealand Journal of Geology and Geophysics* 21: 199–214.

Messadi, A.M., B. Mardassi, J.A. Ouali, and J. Touir. 2016. Sedimentology, diagenesis, clay mineralogy and sequential analysis model of upper Paleocene evaporite–carbonate ramp succession from Tamerza area (Gafsa Basin: Southern Tunisia). *Journal of African Earth Sciences* 118: 205–230.

Metwally, A.A., and K.H. Mahfouz. 2018. The Paleocene/Eocene (P/E) boundary along the eastern plateau of Kharga-Baris oases, Western Desert, Egypt. *Journal of African Earth Sciences* 147: 569–584.

Meunier, A., and A. El Albani. 2007. The glauconite–Fe-illite–Fe-smectite problem: A critical review. *Terra Nova* 19: 95–104.

Miller, K.G., J.D. Wright, M.E. Katz, B.S. Wade, J.V. Browning, B.S. Cramer, and Y. Rosenthal. 2009. Climate threshold at the Eocene–Oligocene transition: Antarctic ice sheet influence on ocean circulation. In *The Late Eocene Earth: Hothouse, Icehouse, and Impacts*, ed. C. Koeberl, and A. Montanari, 452: 169–178. Geological Society of America Special Paper, USA.

Morad, S., J.M. Ketzer, and L.F. De Ros. 2012. Linking diagenesis to sequence stratigraphy: An integrated tool for understanding and predicting reservoir quality distribution. *Linking Diagenesis to Sequence Stratigraphy. Special Publication of the International Association of Sedimentologists* 45: 1–36.

Morton, A.C., R.J. Merriman, and J.G. Mitchell. 1984. Genesis and significance of glauconitic sediments of the southwest Rockall plateau. *Initial Reports of the Deep Sea Drilling Project* 81: 645–652.

Nahon, D., A.V. Carozzi, and C. Parron. 1980. Lateritic weathering as a mechanism for the generation of ferruginous ooids. *Journal of Sedimentary Research* 50: 1287–1298.

Nicolo, M.J., G.R. Dickens, and C.J. Hollis. 2010. South Pacific intermediate water oxygen depletion at the onset of the Paleocene-Eocene thermal maximum as depicted in New Zealand margin sections. *Paleoceanography* 25: Pa4210. https://doi.org/10.1029/2009pa001904.

Nicolo, M.J., G.R. Dickens, C.J. Hollis, and J.C. Zachos. 2007. Multiple early Eocene hyperthermals: Their sedimentary expression on the New Zealand continental margin and in the deep sea. *Geology* 35: 699–702.

Nigam, R., A. Mazumder, P.J. Henriques, and R. Saraswat. 2007. Benthic foraminifera as proxy for oxygen-depleted conditions off the central west coast of India. *Journal of the Geological Society of India* 70: 1047–1054.

Odin, G.S., and A. Matter. 1981. De glauconiarum origine. *Sedimentology* 28: 611–641.

Peters, S.E., and R.R. Gaines. 2012. Formation of the 'great unconformity' as a trigger for the Cambrian explosion. *Nature* 484: 363.

Petters, S.W., and R.K. Olsson. 1979. Planktonic foraminifera from the Ewekoro type section (Paleocene) Nigeria. *Micropaleontology* 25: 206–213.

Pietsch, C., H.C. Harrison, and W.D. Allmon. 2016. Whence the Gosport sand (upper middle Eocene, Alabama)? The origin of glauconitic shell beds in the Paleogene of the US gulf coastal plain. *Journal of Sedimentary Research* 86: 1249–1268.

Polevaya, N.I., G.A. Murina, and G.A. Kazakov. 1961. Utilization of glauconite in absolute dating. *Annals of the New York Academy of Sciences* 91: 298–310.

Porrenga, D.H. 1968. Non-marine glauconitic illite in the lower Oligocene of Aardebrug, Belgium. *Clay Minerals* 7: 421–430.

Poulton, S.W., and D.E. Canfield. 2011. Ferruginous conditions: A dominant feature of the ocean through Earth's history. *Elements* 7: 107–112.

Prasad, V., I.B. Singh, S. Bajpai, R. Garg, B. Thakur, A. Singh, N. Saravanan, and V.V. Kapur. 2013. Palynofacies and sedimentology-based high-resolution sequence stratigraphy of the lignite-bearing muddy coastal deposits (early Eocene) in the Vastan lignite mine, gulf of Cambay, India. *Facies* 59: 737–761.

Raju, S.V., and N. Mathur. 2013. Rajasthan lignite as a source of unconventional oil. *Current Science (Bangalore)* 104: 752–757.

Rasmussen, E.S., and K. Dybkjær. 2005. Sequence stratigraphy of the upper Oligocene–Lower Miocene of eastern Jylland Denmark: Role of structural relief and variable sediment supply in controlling sequence development. *Sedimentology* 52: 25–63.

Rasser, M.W., and W.E. Piller. 2004. Crustose algal frameworks from the Eocene Alpine foreland. *Palaeogeography, Palaeoclimatology, Palaeoecology* 206: 21–39.

Ridgwell, A., and D.N. Schmidt. 2010. Past constraints on the vulnerability of marine calcifiers to massive carbon dioxide release. *Nature Geoscience* 3: 196–200.

Rudmin, M., S. Banerjee, E. Abdullayev, A. Ruban, E. Filimonenko, E. Lyapina, R. Kashapov, and A. Mazurov. 2020. Ooidal ironstones in the Meso-Cenozoic sequences in western Siberia: Assessment of formation processes and relationship with regional and global earth processes. *Journal of Palaeogeography* 9 (1): 1–21.

Rudmin, M., S. Banerjee, and A. Mazurov. 2017. Compositional variation of glauconites in Upper Cretaceous–Palaeogene sedimentary iron-ore deposits in south-eastern western Siberia. *Sedimentary Geology* 355: 20–30.

Rudmin, M., A. Mazurov, and S. Banerjee. 2019. Origin of ooidal ironstones in relation to warming events: Cretaceous–Eocene Bakchar deposit, south-East Western Siberia. *Marine and Petroleum Geology* 100: 309–325.

Sageman, B.B., and R.C. Speed. 2003. Upper Eocene limestones, associated sequence boundary, and proposed Eocene tectonics in eastern Venezuela. In *AAPG Memoir*, ed. C. Bartolini, R.T. Buffler, and J. Blickwede, vol. 79, 1–17.

Saikia, B.K., R.K. Boruah, and P.K. Gogoi. 2009. A X-ray diffraction analysis on graphene layers of Assam coal. *Journal of Chemical Sciences* 121: 103–106.

Samanta, A., M.K. Bera, R. Ghosh, S. Bera, T. Filley, K. Pande, S.S. Rathore, J. Rai, and A. Sarkar. 2013a. Do the large carbon isotopic excursions in terrestrial organic matter across Paleocene–Eocene boundary in India indicate intensification of tropical precipitation? *Palaeogeography, Palaeoclimatology, Palaeoecology* 387: 91–103.

Samanta, A., A. Sarkar, M.K. Bera, J. Rai, and S.S. Rathore. 2013b. Late Paleocene–early Eocene carbon isotope stratigraphy from a near-terrestrial tropical section and antiquity of Indian mammals. *Journal of Earth System Science* 122: 163–171.

Saraswati, P.K., S. Khanolkar, and S. Banerjee. 2018. Paleogene stratigraphy of Kutch, India: An update about progress in foraminiferal biostratigraphy. *Geodinamica Acta* 30: 100–118.

Saraswati, P.K., S. Khanolkar, D.S.N. Raju, S. Dutta, and S. Banerjee. 2014. Foraminiferal biostratigraphy of lignite mines of Kutch India: Age of lignite fossil vertebrates. *Journal of Palaeogeography* 3 (1): 90–98.

Sarma, J.N., and S. Basumallick. 1979. Glauconite in some Eocene carbonate rocks of Mikir hills, Assam. *Indian Journal of Earth Sciences* 6: 186–190.

Sarmah, R.K., and R. Borgohain. 2012. Lithostratigraphy of the Paleogene shelf sediments in Assam and Meghalaya — A review. *Indian Streams Research Journal* 12: 1–4.

Savrda, C.E., J.V. Browning, H. Krawinkel, and S.P. Hesselbo. 2001. Firmground ichnofabrics in deep-water sequence stratigraphy, tertiary clinoform-toe deposits, New Jersey slope. *Palaios* 16: 294–305.

Schiøler, P., K. Rogers, R. Sykes, C.J. Hollis, B. Ilg, D. Meadows, L. Roncaglia, and C. Uruski. 2010. Palynofacies, organic geochemistry and depositional environment of the tartan formation (late Paleocene), a potential source rock in the great South Basin, New Zealand. *Marine and Petroleum Geology* 27: 351–369.

Schmitz, B., B. Peucker-Ehrenbrink, C. Heilmann-Clausen, G. Åberg, F. Asaro, and C.T.A. Lee. 2004. Basaltic explosive volcanism, but no comet impact, at the Paleocene–Eocene boundary: High-resolution chemical and isotopic records from Egypt, Spain and Denmark. *Earth and Planetary Science Letters* 225: 1–17.

Schulte, P., L. Schwark, P. Stassen, T.J. Kouwenhoven, A. Bornemann, and R.P. Speijer. 2013. Black shale formation during the latest Danian event and the Paleocene–Eocene thermal maximum in Central Egypt: Two of a kind? *Palaeogeography, Palaeoclimatology, Palaeoecology* 371: 9–25.

Schweitzer, C.E., V. Ćosović, and R.M. Feldmann. 2005. Harpactocarcinus from the Eocene of Istria, Croatia, and the paleoecology of the Zanthopsidae via, 1959 (Crustacea: Decapoda: Brachyura). *Journal of Paleontology* 79: 663–669.

Self-Trail, J.M., D.S. Powars, D.K. Watkins, and G.A. Wandless. 2012. Calcareous nannofossil assemblage changes across the Paleocene–Eocene thermal maximum: Evidence from a shelf setting. *Marine Micropaleontology* 92: 61–80.

Shiloni, Y., A. Segev, G.M. Martinotti, and M. Raab. 1977. An early Eocene glauconitic bed in hor Hahar, northern Negev, Israel. *Israel Journal of Earth-Sciences* 26: 102–107.

Sluijs, A., L. Van Roij, G.J. Harrington, S. Schouten, J.A. Sessa, L.J. LeVay, G.J. Reichart, and C.P. Slomp. 2014. Warming, euxinia and sea level rise during the Paleocene–Eocene thermal maximum on the Gulf coastal plain: Implications for ocean oxygenation and nutrient cycling. *Climate of the Past* 10: 1421–1439.

Sorrentino, L., J.D. Stilwell, and C. Mays. 2014. A model of tephra dispersal from an early Palaeogene shallow submarine Surtseyan-style eruption(s), the red bluff tuff formation, Chatham Island New Zealand. *Sedimentary Geology* 300: 86–102.

Soudry, D., C.R. Glenn, Y. Nathan, I. Segal, and D. VonderHaar. 2006. Evolution of Tethyan phosphogenesis along the northern edges of the Arabian–African shield during the Cretaceous–Eocene as deduced from temporal variations of Ca and Nd isotopes and rates of P accumulation. *Earth-Science Reviews* 78: 27–57.

Speijer, R.P., and B. Schmitz. 1998. A benthic foraminiferal record of Paleocene Sea level and trophic/redox conditions at Gebel Aweina, Egypt. *Palaeogeography, Palaeoclimatology, Palaeoecology* 137: 79–101.

Sprong, J., T.J. Kouwenhoven, A. Bornemann, C. Dupuis, R.P. Speijer, P. Stassen, and E. Steurbaut. 2013. In search of the latest Danian event in a paleobathymetric transect off Kasserine Island north-Central Tunisia. *Palaeogeography, Palaeoclimatology, Palaeoecology* 379: 1–16.

Stap, L., L.J. Lourens, E. Thomas, A. Sluijs, S. Bohaty, and J.C. Zachos. 2010. High-resolution deep-sea carbon and oxygen isotope records of Eocene thermal maximum 2 and H2. *Geology* 38: 607–610.

Stap, L., A. Sluijs, E. Thomas, and L. Lourens. 2009. Patterns and magnitude of deep sea carbonate dissolution during Eocene thermal maximum 2 and H2, Walvis ridge, southeastern Atlantic Ocean. *Paleoceanography* 24 (1): A1211 https://doi.org/10.1029/2008PA001655.

Stassen, P., E. Thomas, and R.P. Speijer. 2015. Paleocene–Eocene thermal maximum environmental change in the New Jersey coastal plain: Benthic foraminiferal biotic events. *Marine Micropaleontology* 115: 1–23.

Steurbaut, E., C. Dupuis, I. Arenillas, E. Molina, and M.F. Matmati. 2000. The Kalaat Senan section in Central Tunisia: A potential reference section for the Danian/Selandian boundary. *GFF* 122: 158–160.

Steurbaut, E., R. Magioncalda, C. Dupuis, S. Van Simaeys, E. Roche, and M. Roche. 2003. Palynology, paleoenvironments, and organic carbon isotope evolution in lagoonal Paleocene–Eocene boundary settings in North Belgium. In *Causes and Consequences of Globally Warm Climates in the Early Paleogene*, ed. S.L. Wing, P.D. Gingerich, B. Schmitz, and E. Thomas, vol. 369, 291–317. Boulder: Geological Society of America Special Paper.

Strickler, M.E., and R.E. Ferrell Jr. 1990. Fe substitution for Al in glauconite with increasing diagenesis in the first Wilcox sandstone (lower Eocene), Livingston parish, Louisiana. *Clays and Clay Minerals* 38: 69–76.

Tang, D., X. Shi, G. Jiang, X. Zhou, and Q. Shi. 2017b. Ferruginous seawater facilitates the transformation of glauconite to chamosite: An example from the Mesoproterozoic Xiamaling formation of North China. *American Mineralogist* 102: 2317–2332.

Tang, D., X. Shi, J. Ma, G. Jiang, X. Zhou, and Q. Shi. 2017a. Formation of shallow water glaucony in weakly oxygenated Precambrian Ocean: An example from the Mesoprterozoic Tieling formation in North China. *Precambrian Research* 294: 214–229.

Taylor, K.G., and J.H. Macquaker. 2011. Iron minerals in marine sediments record chemical environments. *Elements* 7: 113–118.

Tazaki, K., and W.S. Fyfe. 1992. Microbial green marine clay from Izu-Bonin (West Pacific) deep-sea sediments. *Chemical Geology* 102: 105–118.

Thomas, E. 1998. Biogeography of the late Paleocene benthic foraminiferal extinction. In *Late Paleocene–Early Eocene Climatic and Biotic Events in the Marine and Terrestrial Records*, ed. M.P. Aubry, 214–243.

Tlig, S., S. Sahli, L. Er-Raioui, R. Alouani, and M. Mzoughi. 2010. Depositional environment controls on petroleum potential of the Eocene in the north of Tunisia. *Journal of Petroleum Science and Engineering* 71: 91–105.

Todd, S.E., P.K. Pufahl, J.B. Murphy, and K.G. Taylor. 2019. Sedimentology and oceanography of early Ordovician ironstone, Bell Island Newfoundland: Ferruginous seawater and upwelling in the Rheic Ocean. *Sedimentary Geology* 379: 1–15.

Tóth, E., T.G. Weiszburg, T. Jeffries, C.T. Williams, A. Bartha, É. Bertalan, and I. Cora. 2010. Submicroscopic accessory minerals overprinting clay mineral REE patterns (celadonite–glauconite group examples). *Chemical Geology* 269: 312–328.

van der Lingen, G.J., D. Smale, and D.W. Lewis. 1978. Alteration of a pelagic chalk below a paleokarst surface, Oxford, South Island New Zealand. *Sedimentary Geology* 21: 45–66.

van Houten, F.B. 1992. Review of Cenozoic ooidal ironstones. *Sedimentary Geology* 78: 101–110.

Vanhove, D., P. Stassen, R.P. Speijer, and E. Steurbaut. 2011. Assessing paleotemperature and seasonality during the early Eocene climatic optimum (EECO) in the Belgian Basin by means of fish otolith stable O and C isotopes. *Geologica Belgica* 14: 143–157.

Wei, W. 2004. Opening of the Australia–Antarctica gateway as dated by nannofossils. *Marine Micropaleontology* 52: 133–152.

Wei, W., T.J. Algeo, Y. Lu, Y. Lu, H. Liu, S. Zhang, L. Peng, J. Zhang, and L. Chen. 2018. Identifying marine incursions into the Paleogene Bohai Bay basin lake system in northeastern China. *International Journal of Coal Geology* 200: 1–17.

Wigley, R.A., and J.S. Compton. 2006. Late Cenozoic evolution of the outer continental shelf at the head of the cape canyon, South Africa. *Marine Geology* 226: 1–23.

Zachos, J.C., K.C. Lohmann, J.C. Walker, and S.W. Wise. 1993. Abrupt climate change and transient climates during the Paleogene: A marine perspective. *The Journal of Geology* 101: 191–213.

Zachos, J.C., H. McCarren, B. Murphy, U. Röhl, and T. Westerhold. 2010. Tempo and scale of late Paleocene and early Eocene carbon isotope cycles: Implications for the origin of hyperthermals. *Earth and Planetary Science Letters* 299: 242–249.

Zachos, J.C., M. Pagani, L. Sloan, E. Thomas, and K. Billups. 2001. Trends, rhythms, and aberrations in global climate 65 Ma to present. *Science* 292: 686–693.

Zarasvandi, A., Z. Fereydouni, H. Pourkaseb, M. Sadeghi, B. Mokhtari, and B. Alizadeh. 2019. Geochemistry of trace elements and their relations with organic matter in Kuh-e-Sefid phosphorite mineralization, Zagros Mountain, Iran. *Ore Geology Reviews* 104: 72–87.

Publisher's Note